Title	Rapid, selective heavy metal removal from water by a metal-organic framework/polydopamine composite
Authors	Sun, Daniel T.;Peng, Li;Reeder, Washington S.;Moosavi, Seyed Mohamad;Tiana, Davide;Britt, David K.;Oveisi, Emad;Queen, Wendy L.
Publication date	2018-03-14
Original Citation	Sun, D. T., Peng, L., Reeder, W. S., Moosavi, S. M., Tiana, D., Britt, D. K., Oveisi, E. and Queen, W. L. (2018) 'Rapid, Selective Heavy Metal Removal from Water by a Metal–Organic Framework/ Polydopamine Composite', ACS Central Science, 4(3), pp. 349-356. doi: 10.1021/acscentsci.7b00605
Type of publication	Article (peer-reviewed)
Link to publisher's version	https://pubs.acs.org/doi/10.1021/acscentsci.7b00605 - 10.1021/acscentsci.7b00605
Rights	© 2018 American Chemical Society. This is an open access article published under an ACS AuthorChoice License, which permits copying and redistribution of the article or any adaptations for non-commercial purposes. - https://pubs.acs.org/page/policy/authorchoice_termsofuse.html
Download date	2024-04-24 20:55:30
Item downloaded from	https://hdl.handle.net/10468/5926

Supplementary Materials for

Rapid, Selective Heavy Metal Removal from Water by a Metal-organic Framework/Polydopamine Composite

Authors: Daniel T. Sun[1], Li Peng[1], Washington S. Reeder[1,2], Seyed Mohamad Moosavi[1], Davide Tiana[1], David K. Britt[3], Emad Oveisi[4] and Wendy L. Queen[1*]

Affiliations:

[1]Laboratory for Functional Inorganic Materials, Institute of Chemical Sciences and Engineering, École Polytechnique Fédérale de Lausanne (EPFL), CH-1051 Sion, Switzerland.

[2]Department of Chemical and Biomolecular Engineering, University of California, Berkeley, United States.

[3]The Molecular Foundry, Materials Sciences Division, Lawrence Berkeley National Laboratory, Berkeley, California 94720, United States.

[4]Interdiciplinary Center for Electron Microscopy, École Polytechnique Fédérale de Lausanne (EPFL), CH-1015 Lausanne, Switzerland.

*Correspondence to: wendy.queen@epfl.ch

.

Materials and Methods

Synthesis of Fe-BTC. Iron(III) chloride hexahydrate (97%) was bought from Alfa Aesar and 1,3,5-benzenetricarboxylic acid (trimesic acid, 98%) was bought from ABCR GmbH and used without further purification. All other metal salts and chemicals were bought from Sigma Aldrich and used without further purification. Fe-BTC[19] was prepared using the following synthetic procedure: 9.72 g of iron(III) chloride hexahydrate, 3.36 g of trimesic acid and 120 mL of distilled water were loaded in a 180 mL Teflon autoclave. The reaction mixture was heated to 130 °C for 72 hours. After the reaction was cooled down to room temperature the orange solid was filtered under vacuum and washed with copious amounts of water and methanol. The resulting powder was loaded into a double thickness whatman cellulose extraction thimble and underwent soxhlet purification with methanol for 24 hours. After solvent exchange, the sample was dried under vacuum overnight. The material was activated under vacuum at 150 °C for 17 hours before nitrogen adsorption and standard characterization.

Elemental Analysis Fe-BTC: C 34.65 % H 2.85 % Fe 21.84 % and yield = 4.2 grams

Free Base Dopamine Synthesis. Dopamine HCl, dry sodium hydride 95% and anhydrous solvents were bought from Sigma Aldrich and used without further purification. In a N_2 purged, a 2-neck round bottom flask was charged with 10 g of Dopamine HCl mixed in 80 mL of anhydrous tetrahydrofuran (THF) and 80 mL of anhydrous methanol. 1.264 g of dry sodium hydride 95% was added slowly in small quantities over a period of approximately 15 minutes. The reaction mixture was allowed to stir for 48 hours under flowing N_2. After the completion of the reaction, the mixture was filtered under vacuum and washed with copious amounts of THF. The white powder was dried and kept under vacuum until further use (Supplementary Fig. S1). ^{1}H NMR (400 MHz, Methanol-d_4): δ = 6.72 (d, J = 8.0 Hz, 1H), 6.67 (d, J = 2.1 Hz, 1H), 6.55 (dd, J = 8.0, 2.1 Hz, 1H), 2.87 (t, J = 7.1 Hz, 2H), 2.65 (t, J = 7.1 Hz, 2H).

Fe-BTC/PDA-19 Synthesis. 2 g of Fe-BTC was activated at 150 °C under vacuum overnight in a 500 mL 2-neck round bottom flask using a schlenk line and an oil pump. After activation, the reaction vessel was cooled to room temperature and then N_2 was flowed over the sample for 10 minutes. Afterwards, the sample was sealed under an inert atmosphere. Then 400 mL 0.02 M anhydrous methanol solution containing the as-prepared free base dopamine, was prepared in a glove box purged with N_2. Using a steel cannula and N_2, the methanol/dopamine solution was transferred to the flask containing the activated Fe-BTC. Over a period of 1 hour, the orange powder turned dark purple indicative of polymerization. The reaction was allowed to stir for 24 hours at room temperature under an inert atmosphere. After completion, the reaction mixture was filtered under vacuum and washed with copious amounts of methanol and water. To remove any excess dopamine, the resulting purple powder was loaded into a double thickness Whatman cellulose extraction thimble, and the composite underwent soxhlet extraction with methanol for 24 hours under N_2. Afterwards, the sample was dried under vacuum at room temperature over night, and then the material was activated under vacuum at 125 °C for 17 hours before nitrogen adsorption and standard characterization was carried out.

Elemental Analysis Fe-BTC/PDA-19: C 39.553% N 1.81% H 2.45% Fe 17.84%

It should be noted that several samples were prepped with various loadings of dopamine. The amount of dopamine loaded into the MOF was altered by varying the concentration of free dopamine in methanol before its addition to an activated Fe-BTC sample. Five Fe-BTC/PDA samples were prepped including, Fe-BTC/PDA-19, Fe-BTC/PDA-28, Fe-BTC/PDA-38 and Fe-

BTC/PDA-42. The dopamine concentrations in 400mL of methanol were varied from 12 mM, 24 mM, 36 mM and 47 mM, respectively.

Powder X-Ray Diffraction. Synchrotron powder x-ray diffraction data was collected at BM31 at the Swiss-Norwegian Beam Line (SNBL) of ESRF using a wavelength of 0.50084 Å. Samples were loaded into 0.9 mm borosilicate capillaries and activated using a custom built manifold and turbo pump. After activation the capillaries were flame sealed and loaded onto a goniometer and spun. The diffraction patterns were collected using a 2D MAR345 image plate detector at a distance of 0.3584 mm for 60 seconds. The resulting images were integrated using the FIT2D program (*47*). Lab Source powder x-ray diffraction was performed on a Bruker D8 Discover system with a Cu K Kα source (1.54056 Å) at 40kV and 40 mA. The powder samples were loaded and flattened onto a zero background sample holder. The scanning range was 1-30° over 1500 steps at a scanning rate of 1 step per second. Simulated powder patterns were generated using Mercury 3.6 crystallography software.

Nitrogen Adsorption Measurements. For all gas adsorption measurements, samples ranging from 100-200 mg were transferred to a pre-weighed glass sample tube. The samples were degassed under vacuum at 125 °C for 15 hours at a ramp rate of 1.0 °C per minute. After activation, the samples were cooled to room temperature, back filled with argon, and transferred to a Belsorp-max gas adsorption analyzer. All adsorption experiments were performed at 77 K using liquid N_2. For N_2 adsorption isotherms, 99.999% purity gas was used. After the isotherms were generated the surface areas (m^2/g) were calculated using the BET (Brunaer-Emmet-Teller) method.

X-ray Photoelectron Spectroscopy. X-ray photoelectron spectroscopy measurements were carried out using a Physical Instruments AG PHI VersaProbe II scanning XPS microprobe. Analysis was performed using a monochromatic Al Kα X-ray source of 24.8 W power with a beam size of 100 μm. The spherical capacitor analyzer was set at 45° take-off angle with respect to the sample surface. The pass energy was 46.95 eV yielding a full width at half maximum of 0.91 eV for the Ag 3d 5/2 peak.

Electron Microscopy Measurements. Energy dispersive x-ray (EDX) spectroscopy and electron energy loss spectroscopy (EELS) were performed on a FEI Titan Themis 60-300 in scanning transmission electron microscopy mode (STEM) at an accelerating voltage of 200 kV. This microscope is equipped with a high brightness X-FEG gun and silicon drift Super-X EDX detectors, and a Gatan GIF Quantum ERS spectrometer. Images were acquired using a high-angle annular dark-field (HAADF-STEM) detector with 23–200 mrad collection angle. STEM-EDX elemental maps were acquired using a beam current of ~250 pA. Sample preparation for STEM measurements was done using ultramicrotomy. A resin-embedded composite was serially sectioned in ~100 nm thick slices that were deposited on a TEM grid with an ultrathin carbon support film.

Batch Heavy Metal Removal Experiments. Fe-BTC and Fe-BTC/PDA removal capacities were compared at varying concentrations. Different concentrations of Pb^{2+} ($Pb(OAc)_2$) and Hg^{2+} ($HgCl_2$) salts were prepared using distilled water, water from the Rhone river (Sion, Switzerland, Latitude: 46.228332, Longitude: 7.369975) and water from the Mediterranean Sea (Nice, France, Latitude: 43.694937, Longitude: 7.276565). About 10 mg of Fe-BTC or Fe-BTC/PDA-19 were added to 20 mL of the solution and the vials were placed in a Thermo Scientific MaxQ4450 Orbital Shaker for 24 hours at 200 rpms and held at a constant temperature of 28 °C. The samples were filtered using a 25 mm hydrophilic PTFE membrane syringe filter with 0.22 μm

pores to remove any solids and elemental analysis was carried out on the remaining aqueous media. After the analysis, Q_e, the amount of metal removed per gram of composite (mg/g), was calculated using the following equation:

$$Q_e = \frac{C_o V - C_e V}{m}$$

where, C_o is the initial concentration, C_e is the end concentration, V is the volume of the simulated contaminated water, and m is the mass of the composite

Rate of Removal Experiment. Various vials containing 20 mL of 1 ppm millipore water solutions of Hg^{2+} or Pb^{2+} were treated with ~20 mg of Fe-BTC or Fe-BTC/PDA. At each time point, the samples were filtered using a 25 mm hydrophilic PTFE membrane syringe filter with 0.22 μm pores to remove any solids for elemental analysis of the aqueous media. After analysis, the percent removal was calculated using the following equation:

$$Percent\ Removal\ \% = \frac{C_o - C_e}{C_o} x100$$

Regeneration. Regeneration of the materials was investigated using reagents such as EDTA (ethylenediaminetetraacetic acid) for the desorption of Pb^{2+} and ascorbic acid for the reduction of the quinones to the catechols in polydopamine in the case of Hg^{2+}. For this experiment, 0.500 g of Fe-BTC/PDA-19 was added to 1000 ppm 1 liter aqueous solutions of Pb^{2+} and Hg^{2+} to saturated the samples. After 24 hours, the samples were filtered, dried, and weighed. The Pb^{2+} and Hg^{2+} concentrations in the aqueous media were analyzed and the values were used to calculate the capacity value Q_e (mg/g). The samples were added to 0.001M solutions of EDTA and Ascorbic acid and allowed to shake at 200 rpms for 4 hours. The samples were filtered, washed with methanol, dried and weighed. The EDTA regeneration solution was made into a 2 % HNO_3 solution for analysis to obtain the Pb^{2+} concentration to calculate the % recovery of Pb^{2+}. The regenerated materials were then added to 1000 ppm solutions of Pb^{2+} and Hg^{2+}. This procedure was repeated 3 more times to obtain the capacity Q_e (mg/g) for each of the 4 cycles.

H^1 NMR of Free Base Dopamine

Free base dopamine was dissolved in deuterated methanol and analyzed using a Bruker AVDHD 400 MHz 9.5 T NMR and a 5 mm BBFO liquid probe. After 128 scans, the proton NMR spectrum was integrated using Maestro NMR analysis software[23].

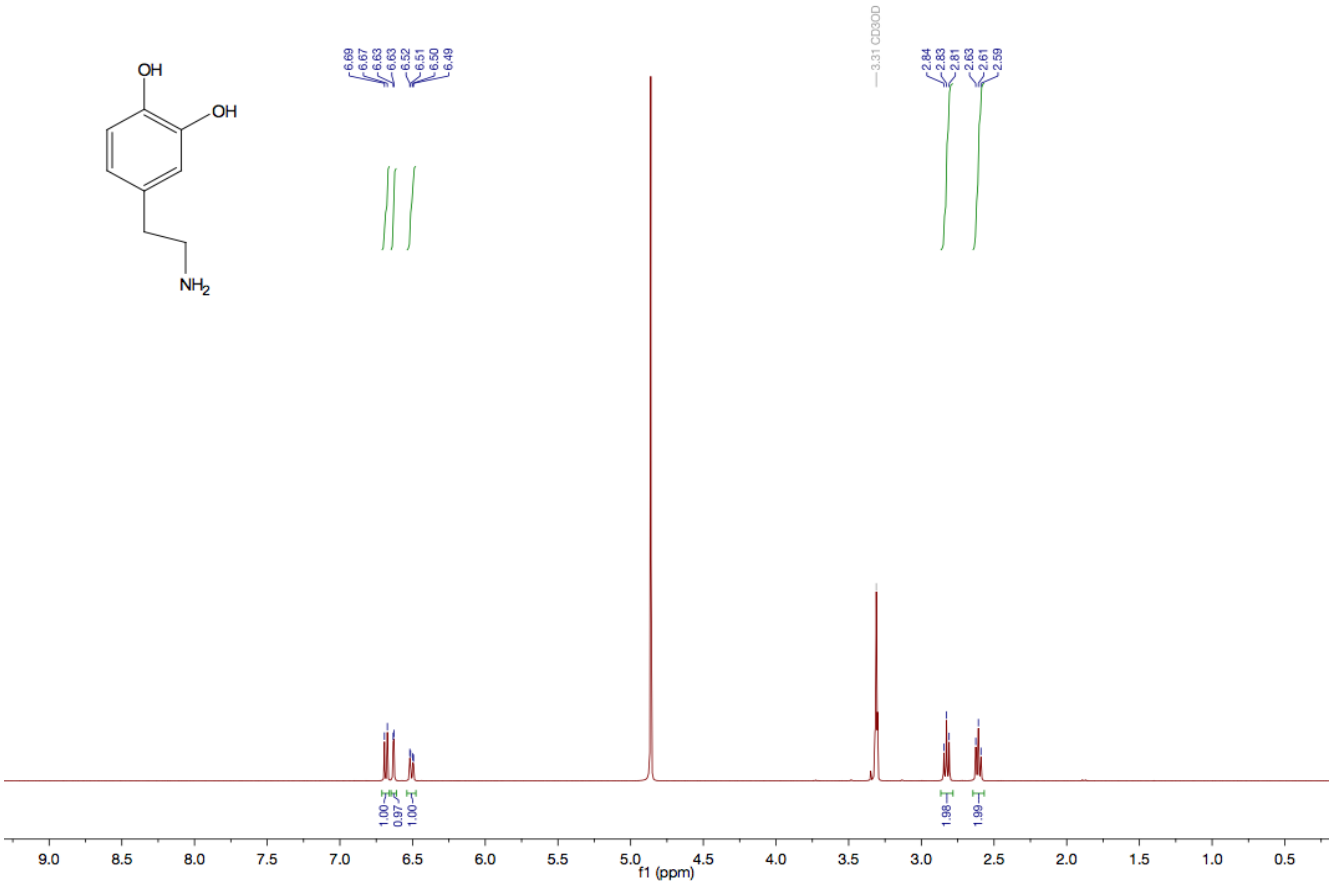

Figure S1 | ^{1}H NMR spectrum of the as synthesized free base dopamine.

In-Situ FT-IR with CO

In-situ IR data was collected in transmission mode on samples mounted on a self-supported wafer using a custom-built infrared cell and a Harrick Scientific Praying Mantis on a PerkinElmer Frontier Spectrometer at -123 °C. Before measurements, the samples of Fe-BTC and Fe-BTC/PDA were activated overnight at 150 °C and 125 °C, respectively, while all under dynamic vacuum. After cooling down, the sample cell was purged with Argon for half an hour and then cooled to -123 °C. The background was collected and CO was then charged into the sample cell. The background subtracted *in-situ* DRIFTS spectra were collected for Fe-BTC/PDA-42, Fe-BTC/PDA-38, Fe-BTC/PDA-28, Fe-BTC/PDA-19, and Fe-BTC at -123 °C (with a CO equilibrium pressure of 125, 46, 173, 103, and 650 mbar respectively). The observed changes in intensity with increased dopamine loading imply that the metal sites are being blocked by polymer.

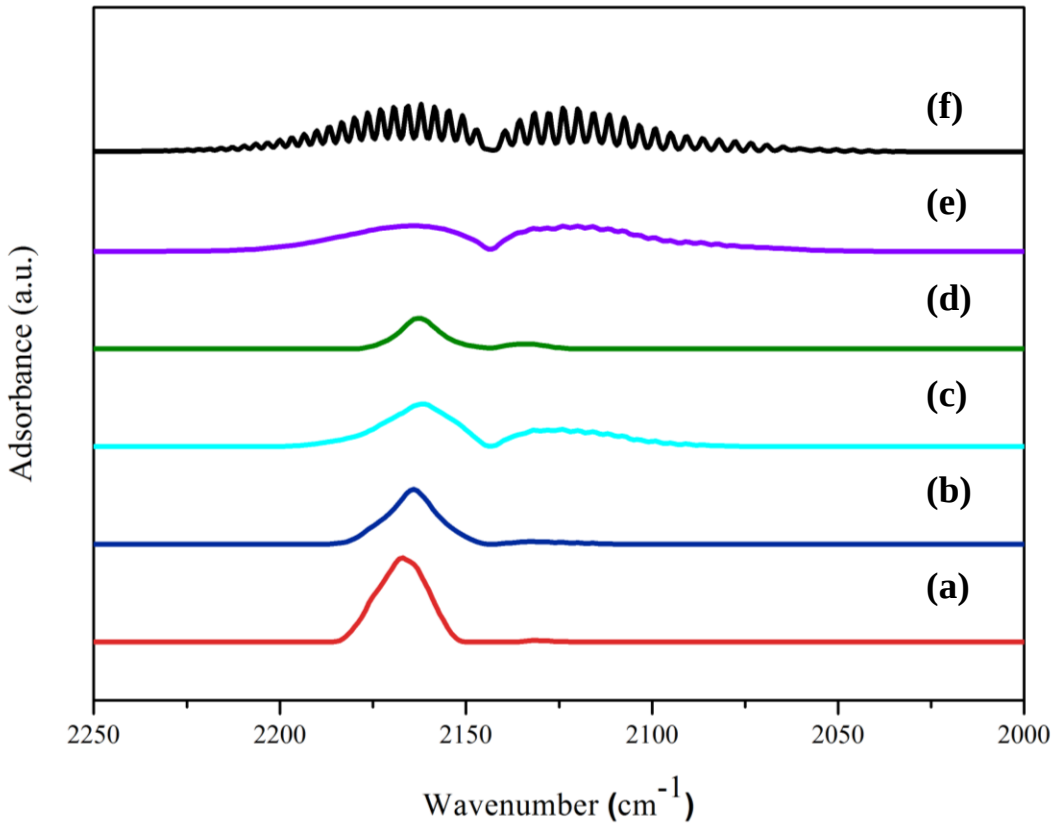

Figure S2 I *In-situ* FT-IR drift with CO. (a) Fe-BTC (b) Fe-BTC/PDA-19 (c) Fe-BTC/PDA-28 (d) Fe-BTC/PDA-38 (e) Fe-BTC/PDA-42 (f) Free CO

Long-term stability of Fe-BTC/ PDA

Stability of Fe-BTC/PDA was assessed using synchrotron powder x-ray diffraction, MALDI and ICP-OES. Samples were first soaked in water from the Rhone River with and without lead and mercury contamination (approximate concentration = 1 and 1000 ppm) for 8 weeks at room temperature. The solutions were centrifuged at 7000 rpms and the isolated solids were dried overnight under vacuum. MALDI (see Fig. S6 for methods) analysis was done on the Rhone river water and Rhone river water with Fe-BTC/PDA to see if any polymer was leaching into solution. The MALDI spectra show no evidence of PDA in Rhone River water.

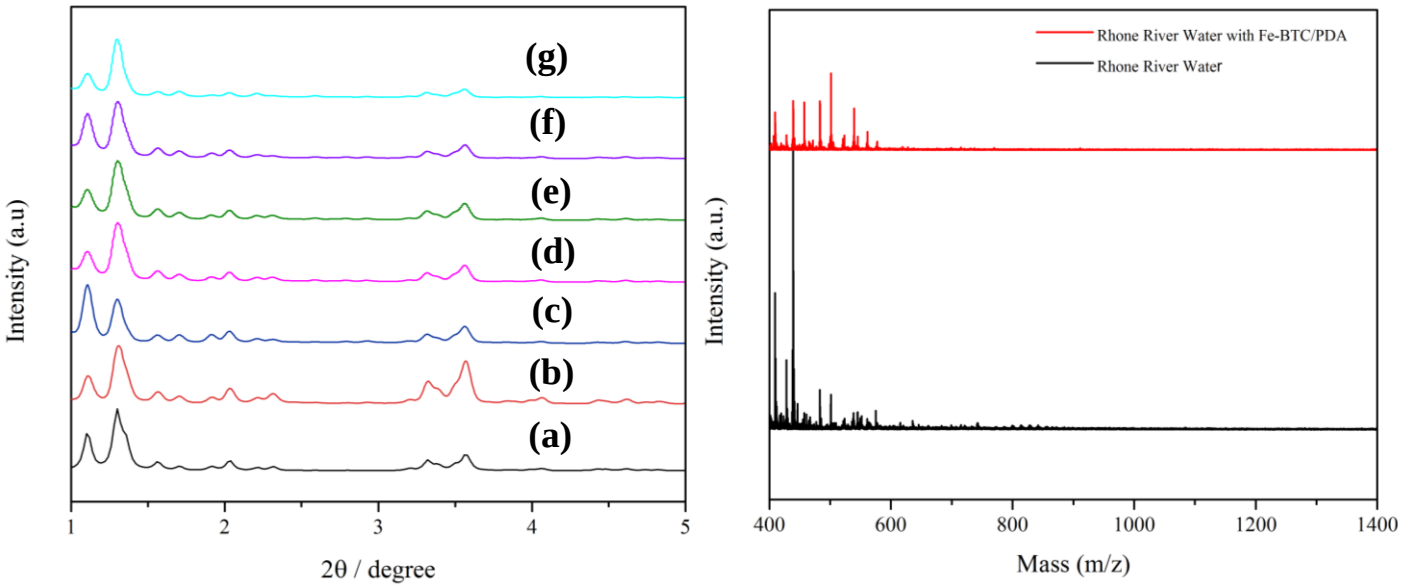

Figure S3 | (left) Powder X-ray diffraction of (a) simulated, (b) Fe-BTC/PDA-19, (c) Fe-BTC/PDA-19 in river water, (d) Fe-BTC/PDA-19 in a 1 ppm Hg^{2+} solution, (e) Fe-BTC/PDA-19 in a 1 ppm Pb^{2+} solution, (f) Fe-BTC/PDA-19 in a 1000 ppm Hg^{2+} solution and (g) Fe-BTC/PDA-19 in a 1000 ppm Pb^{2+} solution. MALDI spectra (right) of Rhone River water (black) and Rhone River water with Fe-BTC/PDA soaked for 8 weeks illustrating no polymer leaching.

Attenuated Total Reflection Infrared Spectroscopy

ATR-IR spectra were collected using a Perkin-Elmer Frontier MIR/FIR spectrometer equipped with a Quest ATR attachment. The sample was pressed on a diamond window and the spectra were recorded between 4000 and 400 cm^{-1} at a resolution of 4 cm^{-1}. Three new peaks are observed for Fe-BTC/PDA compared to Fe-BTC. These signature stretches emerge at 1273 cm^{-1}, 806 cm^{-1} and 570 cm^{-1} and represent the C–O, C–N and O–H stretching modes in the polymer, respectively

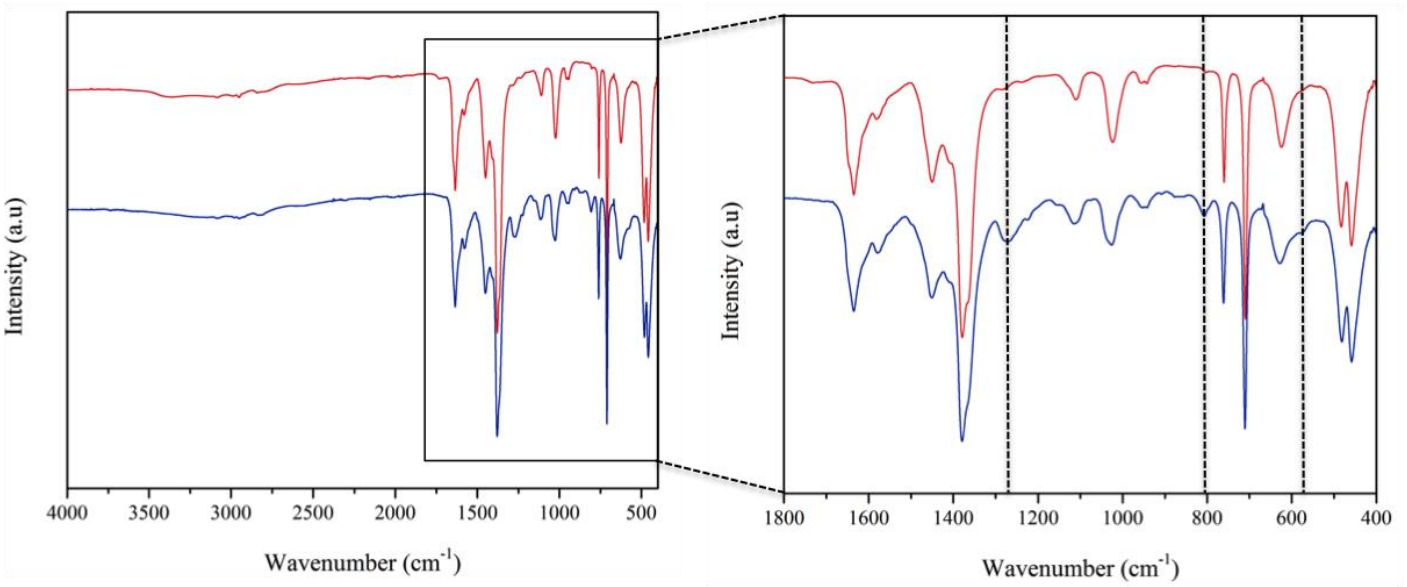

Figure S4 | IR-ATR spectrum of Fe-BTC (red) and Fe-BTC/PDA-19 (blue).

Thermogravimetric Analysis

The thermogravimetric analysis curve was obtained using a TA Q-Series TGA Q500. Samples were loaded onto a tared platinum pan. The balance flow rate was at 10 mL/min with nitrogen and the sample flow rate was at 25 mL/min with air heating at a rate of 1 °C per minute. The TGA for Fe-BTC/PDA illustrates a similar curve compared to Fe-BTC as well. The composite starts degrading at 250 °C and we observed a higher weight lost on the final transition indicating that we have added more organics to the system.

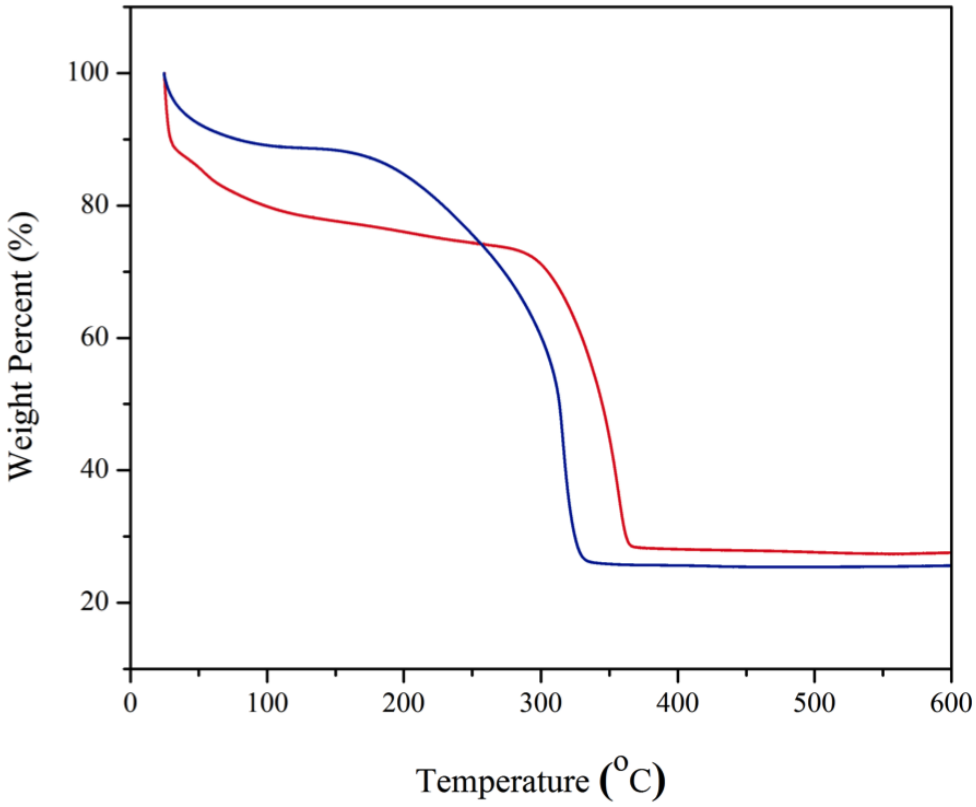

Figure S5 I Thermogravimetric analysis curve of Fe-BTC (red) and Fe-BTC/PDA-19 (blue). The ramp rate was 1 °C per minute.

Polymer Characterization

Matrix-assisted laser desorption/ionization time of flight mass spectrometry (MALDI-TOF-MS) analysis was performed using a Bruker Microflex. 50 mg of Fe-BTC, Fe-BTC/PDA-19 and Fe-BTC/PDA-42 were soaked in 4M HCl solution (15 mL) and then 5 mL of methanol were added to the solution to dissolve the ligand. Then 1uL of the solutions were mixed with the following matrix: 1 uL of 2,5-dihydroxybenzoic acid H_2O/Acetonitrile/Trifluoroacetic acid (49.9/50/.1), and then the solutions were dried on a sample plate. The mode was set to linear with a positive polarity. The MALDI spectra of Fe-BTC/PDA-19 and Fe-BTC/PDA-42 illustrate the presence of PDA in solution that consists of as many as 7 monomeric units.

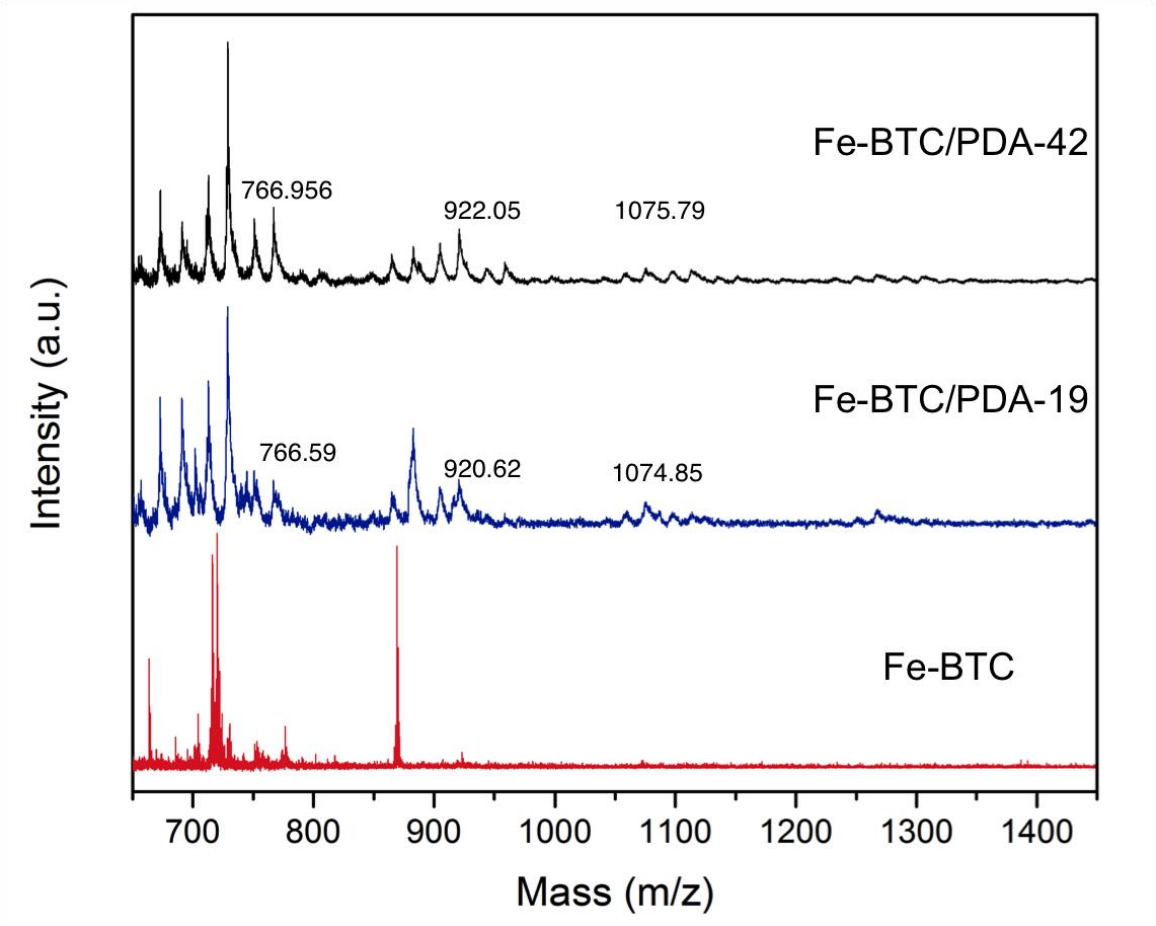

Figure S6 | MALDL-TOF-MS spectra of Fe-BTC, Fe-BTC/PDA-19 and Fe-BTC/PDA-42 after destroying the materials in 4M HCl. The results indicate the polymerization of dopamine.

Scanning Electron Microscopy

Scanning Electron Microscopy (SEM) analysis was performed on a FEI Teneo at an accelerating voltage of 1.0 kV using a beam current of 13 pA. SEM images were acquired with an in-column (Trinity) detector. To minimize electron-charging effects, samples were sputter-coated with iridium (~ 7 nm thick) in a Quorum-Q150.

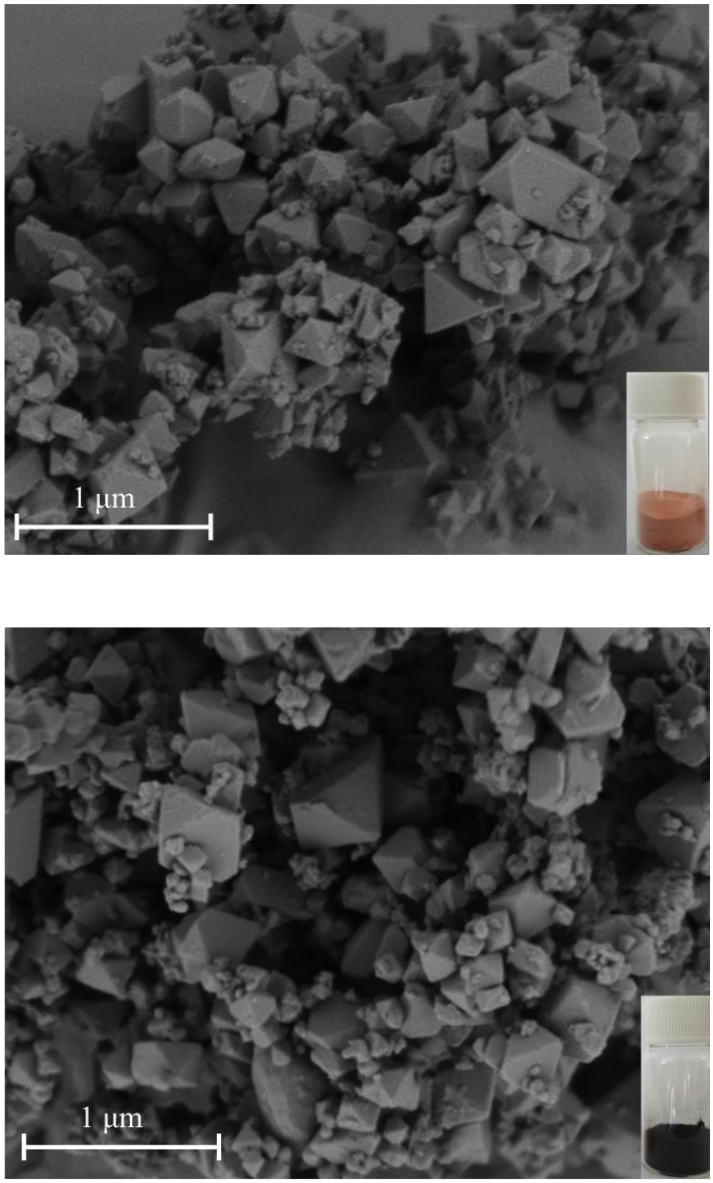

Figure S7 | SEM images of Fe-BTC (top) and Fe-BTC/PDA-19 (bottom).

STEM-Electron-Dispersive X-ray Specytoscopy

Fe-BTC/PDA-19 was embedded in an epoxy resin and serially cut into 100 nm slices and deposited onto a TEM grid (see Methods) for elemental analysis using EDX.

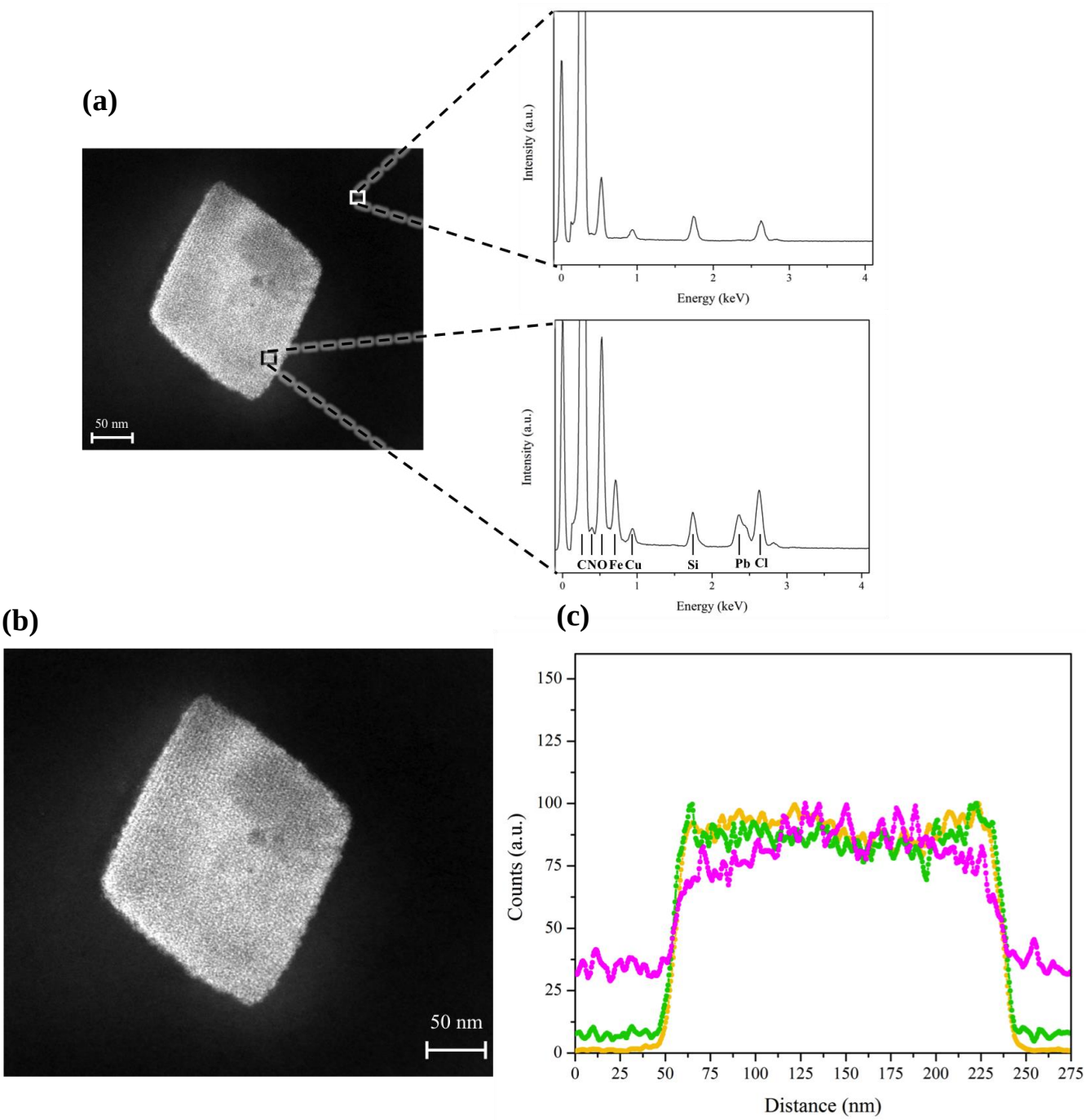

Figure S8 | (a) HAADF-STEM image coupled with EDX spectra of the substrate and an Fe-BTC/PDA-19 crystallite. (b) Scanning transmission electron microscopy images coupled with (c) energy-dispersive X-ray spectroscopy (collected for 1 hour) reveals the presence of Fe (yellow), N (purple) and Pb (green) along a 275 nm line across the Fe-BTC/PDA-19 crystallite.

STEM– Electron Energy Loss Spectroscopy

STEM-EELS measurements were done with a beam current of ~ 250 pA and mapping was performed using the "ultrafast" spectrum imaging mode over a region of 126 x 80 pixels and with a dwell time of 0.25 ms per pixel.

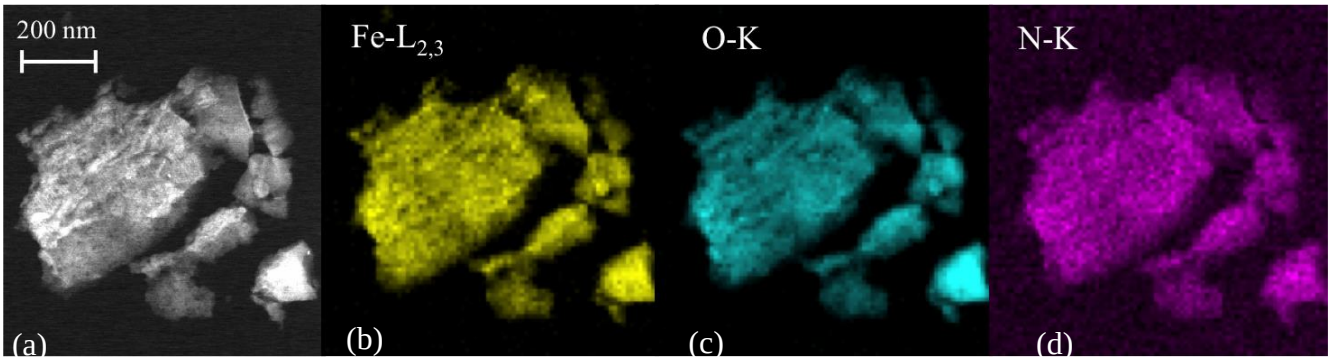

Figure S9 | (a) HAADF-STEM image and corresponding EELS color-coded element mapping of (b) Fe, (c) O, and (d) N in selected Fe-BTC/PDA-19 particles.

Density Functional Theory Calculations

Density functional theory (DFT) calculations were used to elucidate the interactions between Fe-BTC and polydopamine. Since the unit cell of Fe-BTC is excessively large for periodic DFT calculations, we performed the calculations on a fragmented cluster of the MOF (Fig. S10). The structure of PDA is still under debate[26-27], therefore we chose a representative set of all possible structures (monomers) of PDA to investigate the feasible binding configurations of the polymer to the MOF internal surface (Table S2). In principle, the confined ligand environment alongside the Fe(III) open metal site can restrict the polymer confirmation. Consequently, for each structure in the set, additional aromatic unit(s) were appended to the PDA structure to mimic the steric effects of bulky polymer inside the confined pore. The energies were calculated using a plane wave basis set and projector augmented wave (PAW) pseudopotential as implemented in the Quantum-ESPRESSO package with PBEsol exchange-correlation functional and DFT-D2 corrections[28-29], which have shown good accuracy for metal-organic frameworks[30-32]. The simulation box size was set to 30 Å ensuring isolated molecule simulation. In all calculations, the electronic structures were optimized using spin-polarized calculation at gamma point only and using a kinetic energy cutoff of 500eV or higher. Spin polarized calculations were performed optimizing the total magnetization of the system. The cluster of Fe-BTC and the PDA structures were optimized separately to calculate the ground state total energy of each derivative. Afterwards, each PDA structure was placed inside the simulation box together with the MOF cluster. The initial configuration illustrates that the binding site of the PDA structure is attracted to one of the open metal sites (Fig. S10). The Fe-BTC SBU's atoms were kept fixed from the previous optimized step whilst the PDA derivative was relaxed. In all structural optimizations, the quasi-Newtonian relaxation algorithm was used to reach convergence threshold for the total forces and energies lower than 0.5 kcal/mol. Å and 0.1 kcal/mol, respectively. The binding

energies of each configuration were determined as the difference between the energy of later step and former one, as shown in the equation below.

$$\Delta E_{binding} = E_{MOF+PDA} - E_{MOF} - E_{PDA}$$

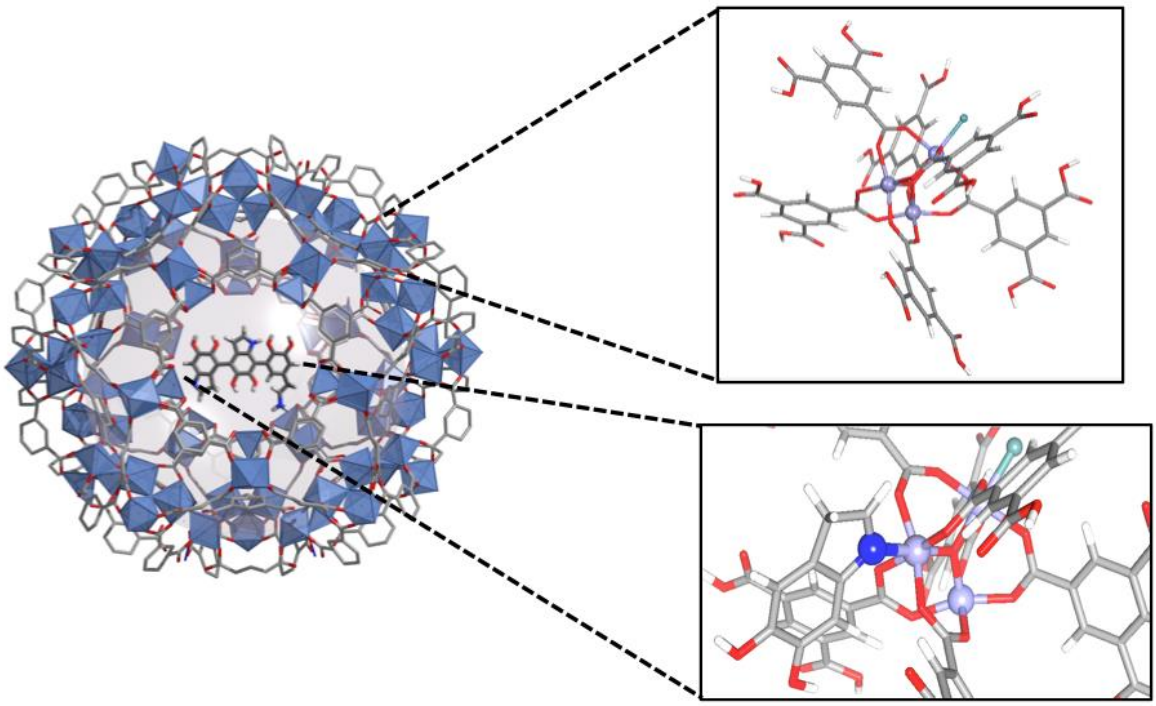

Figure S10 | DFT calculations were carried out on a fragmented cluster of the MOF (top box). The binding energies and bond distances were calculated for various possible polydopamine structures. The values are represented in Table S2.

Raman and ATR-IR

ATR-IR was performed using the methods mentioned above. Raman spectroscopy was carried out using a Renishaw microscope, where the focused excitation light is collected in a back scattering configuration. The powder sample is loaded onto a translational stage of a Leica microscope equipped with a 50x objective, and the excitation is a laser diode of 633 nm at 1% power (115 μW) to prevent degradation of the sample. The spectra were collected from 400 cm^{-1} to 900 cm^{-1} with a 25 second acquisition time. All experiments were conducted at room temperature and in air. Peaks associated with the polymer interacting with the Fe^{3+} along the pore surface are observed in both spectroscopy experiments shown below.

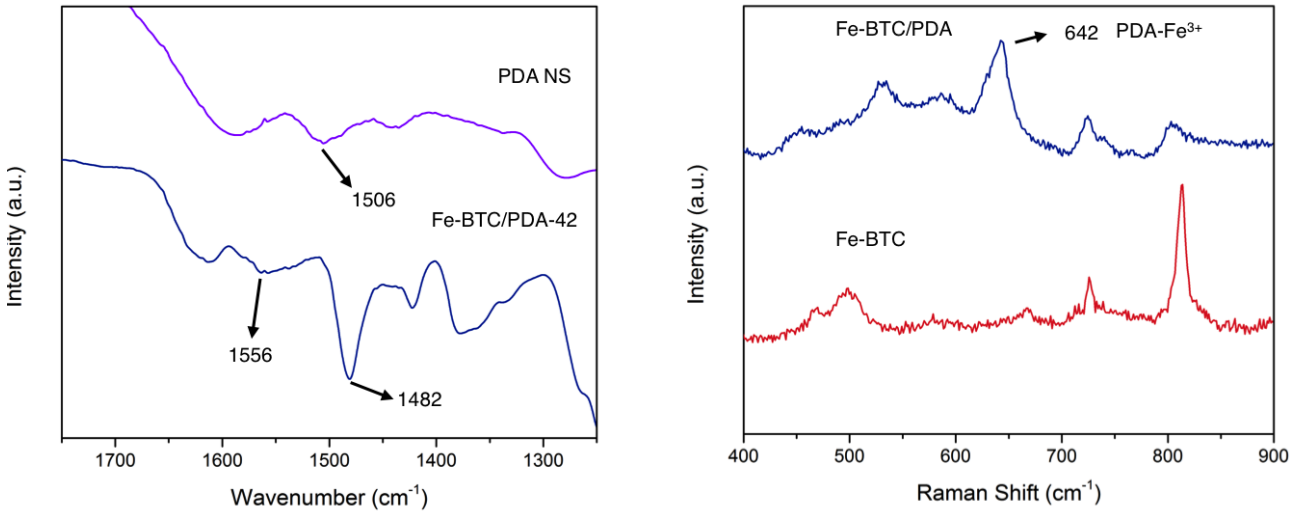

Figure S11 | ATR-IR spectra (left) of PDA nanospheres (purple) and FeBTC/PDA-42 (blue) and Raman Spectra (right) of Fe-BTC (red) and Fe-BTC/PDA-42 (blue).

Prussian Blue Test

Colorimetric Prussian blue tests were performed on the bare framework and the composite (Fig. S10). The a 10 mL aqueous solution was created by mixing 1 mg of $FeCl_3$ and 2 mg of $K_3Fe(CN)_6$ giving a yellow liquid. Roughly 5 mg of Fe-BTC and Fe-BTC/PDA-19 were added to separate 1 mL solutions with Fe-BTC/PDA-19 solution turning blue instantly indicative of free catechols present. Fe-BTC and Fe-BTC/PDA soaked in a Hg^{2+} solution gave negative results.

Figure S12 | Prussian blue test of Fe-BTC (left) and Fe-BTC/PDA-19 (middle) and FeBTC/PDA-19 soaked in a Hg solution (right). The change in color from yellow to blue illustrates free catechols throughout the composite.

Initial Screening for Removal of Hg, Pb, As, Cr, and Cd

Fe-BTC and Fe-BTC/PDA-19 were screened in water solutions containing the nefarious five (Hg, Pb, As, Cr, Cd). First, 1 ppm solutions were prepared for each of the metal salts. Next, ~10 mg of Fe-BTC or Fe-BTC/PDA-19 were added to 20 mL of the aforementioned solutions. The vials were placed in a Thermo Scientific MaxQ4450 Orbital Shaker for 24 hours at 200 rpms and held at a constant temperature of 28°C. The samples were filtered to remove any solid for subsequent elemental analysis of the aqueous media. Fe-BTC/PDA-19 illustrates a significance increase in capacities for all cases except hexavalent chromium and reduces the concentration of Hg^{2+} and Pb^{2+} to drinkable levels below the EPA limit respectively. As such, Hg^{2+} and Pb^{2+} were chosen for further investigation.

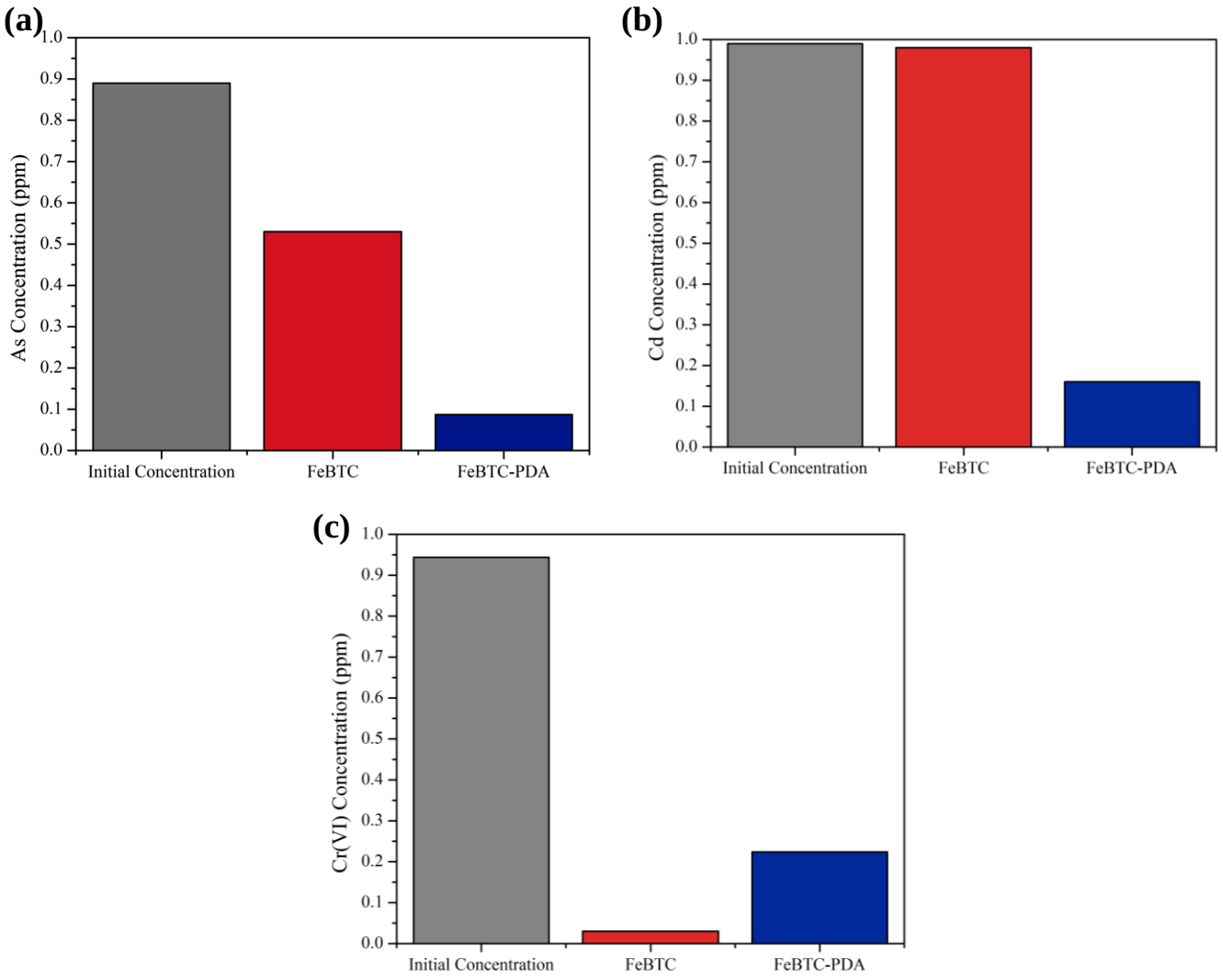

Figure S13 | Screening of the nefarious five, (a) As, (b) Cd, or (c) Cr. Approximately 1 ppm solutions were treated with Fe-BTC (red) and Fe-BTC/PDA-19 (blue). The concentrations were measured before (grey) and after treatment with the bare framework and the composite.

Kinetic Model

Various vials containing 20 mL of 1.8 ppm millipore water solutions of Pb^{2+} were treated with ~20 mg of Fe-BTC/PDA between 0 and 60 seconds. At each time point, the samples were filtered using a 25 mm hydrophilic PTFE membrane syringe filter with 0.22 μm pores to remove any solids for elemental analysis of the aqueous media. Experimental data was fitted with a pseudo-second-order kinetic model[33] shown below.

$$\frac{t}{q_t} = \frac{1}{k_2 q_e^2} + \frac{t}{q_e}$$

where, k_2 (g mg^{-1} min^{-1}) is the rate constant, q_t (mg/g) is the amount adsorbed at time (min) and q_e (mg/g) is the amount adsorbed at equilibrium). The R^2 value of 0.99998 was obtained. The rate constant k_2 was calculated to be 216.7 g mg^{-1} min^{-1}.

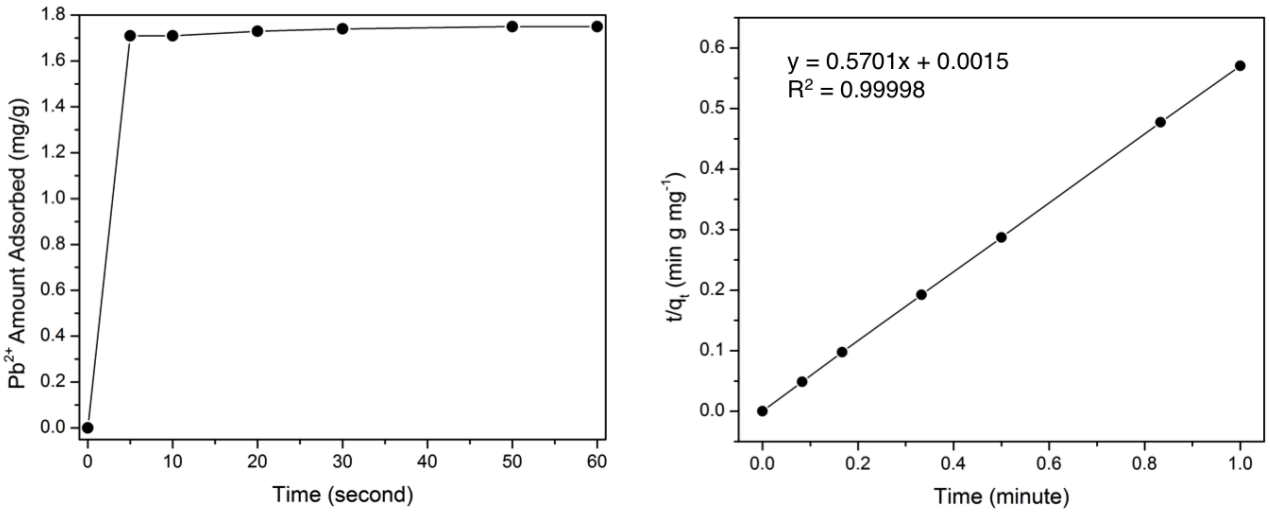

Figure S14 | Adsorption kinetics of Pb^{2+} between 0 and 60 seconds (left) obtained from a starting concentration of 1.8 ppm. The data was fit using a pseudo-second-order kinetic model (right).

Batch Adsorption Experiments

Fe-BTC and Fe-BTC/PDA were soaked in distilled water and Rhone River water spiked with varying concentrations of Hg^{2+} and Pb^{2+} (See methods for experimental details). We observe an enhancement for Fe-BTC/PDA's ability to reduce the concentration of heavy metals compared to Fe-BTC.

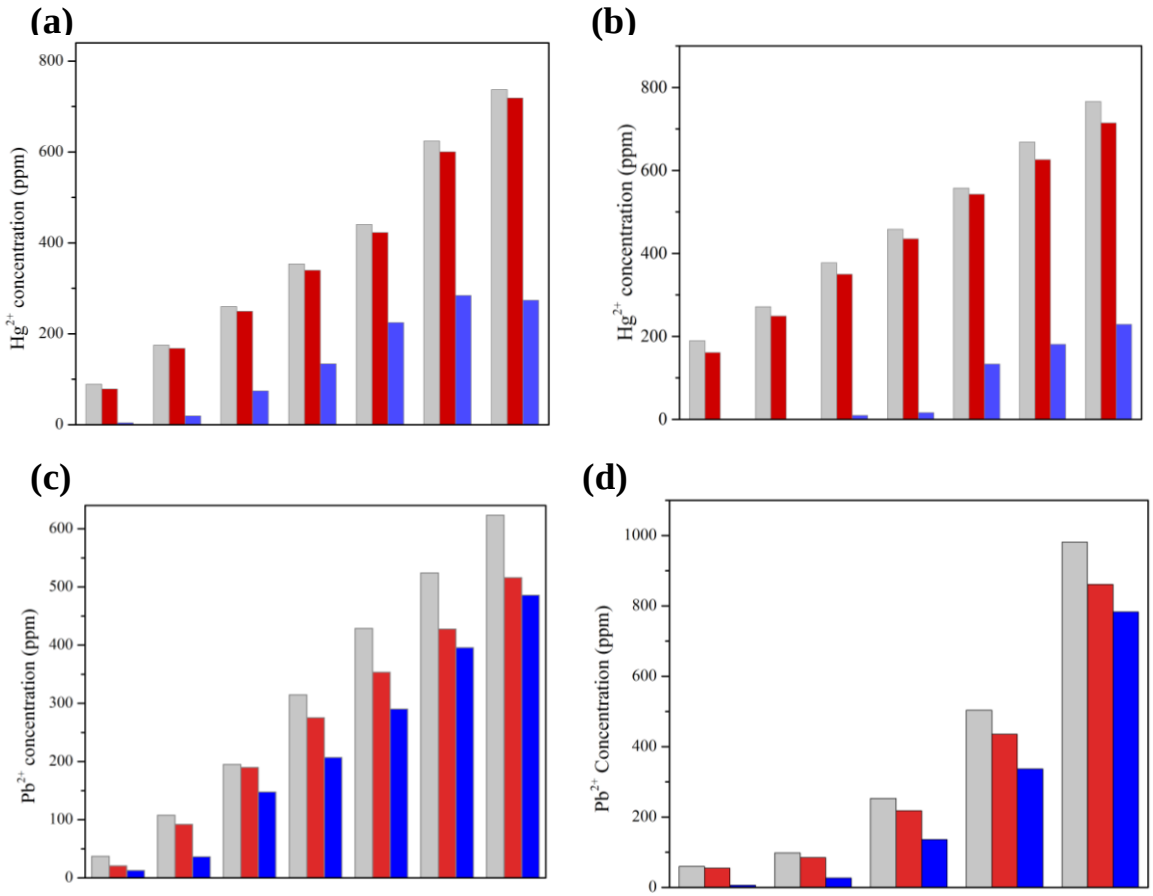

Figure S15 | Batch capacity experiments illustrating the removal of Hg^{2+} from (a) distilled water and (b) Rhone River water and Pb^{2+} from (c) distilled water using FeBTC (red) and Fe-BTC/PDA-19 (blue). Batch capacity experiments illustrating the removal of Pb^{2+} from (d) distilled water using Fe-BTC (red) and Fe-BTC/PDA-42 (blue). The grey bars represent the starting concentration of mercury or lead.

$k_{d,}$ Distribution Coefficient

We obtained the k_d values by immersing and shaking 10 to 45 mg of Fe-BTC/PDA-19 in 1 ppm 1000 mL and 500 mL aqueous solutions of Pb^{2+} and Hg^{2+} at 200 rpms and at a temperature of 28 °C for 24 hours. The samples were filtered using a 25 mm hydrophilic PTFE membrane syringe filter with 0.22 μm pores to remove any solids for elemental analysis of the aqueous media. After the analysis, k_d, the distribution coefficient was calculated using the follow equation:

$$k_d = \frac{C_o - C_e}{C_e}\left(\frac{V}{m}\right)$$

where, C_o is the initial concentration, C_e is the end concentration, V (mL) is the volume of the solution and m (g) is the mass of the composite.

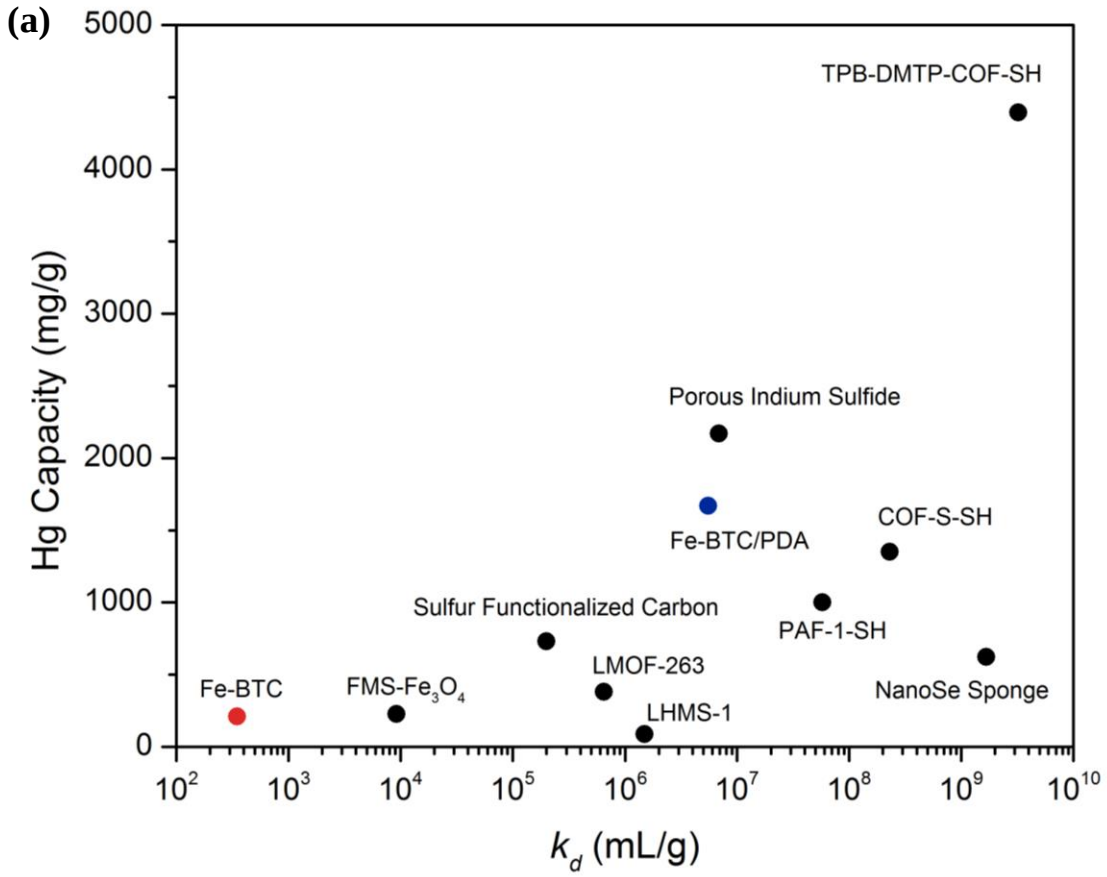

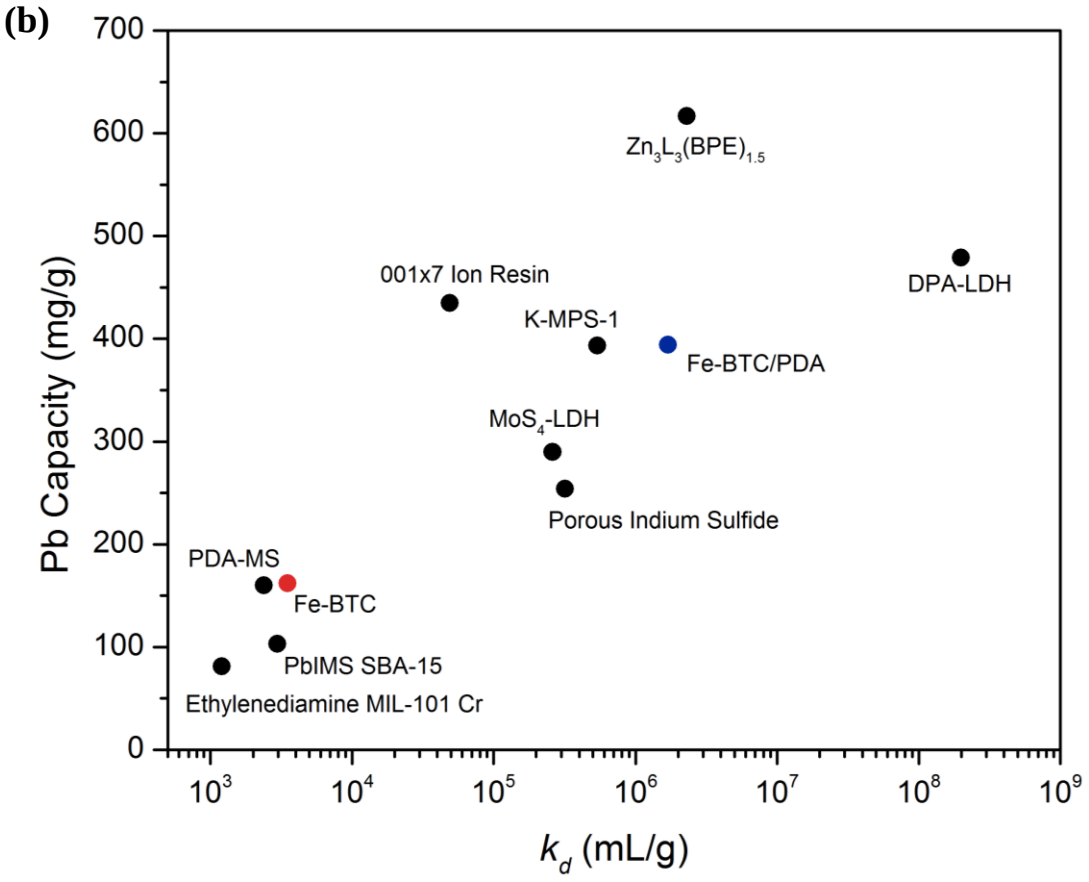

Figure S16 | The calculated distribution coefficient value, k_d and removal capacities of Fe-BTC/PDA in (a) Hg^{2+} and (b) Pb^{2+} solutions are compared to those of other benchmark materials[1-18].

Heavy Metal Removal Experiments with humic acid

The quality of the material was tested in the presence of a common organic interferent, humic acid. Solutions with Pb^{2+} and Hg^{2+} concentrations ranging from 200 to 900 ppm and approximately 100 ppm of humic acid were prepared using distilled water. About 10 mg of Fe-BTC/PDA-19 or Fe-BTC/PDA-42 were added to 20 mL of the solution and the vials were placed in a Thermo Scientific MaxQ4450 Orbital Shaker for 24 hours at 200 rpms and held at a constant temperature of 28 °C. The samples were filtered using a 25 mm hydrophilic PTFE membrane syringe filter with 0.22 µm pores to remove any solids for elemental analysis of the aqueous media.

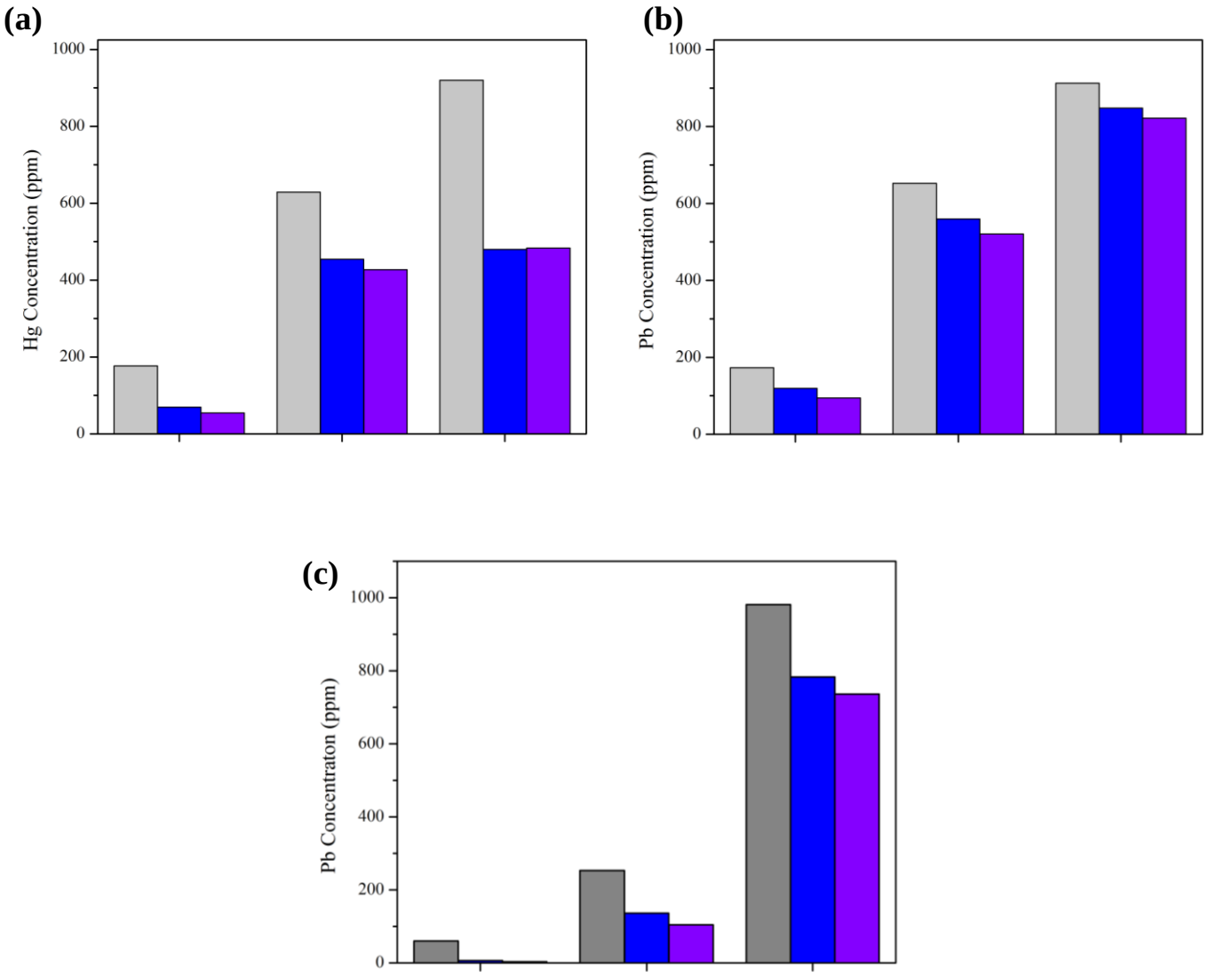

Figure S17 | Bar plots showing (a) Hg^{2+} and (b-c) Pb^{2+} removal from distilled water and distilled water spiked with 100 ppm humic acid. Plots (a) and (b) were treated with Fe-BTC/PDA-19 while plot (c) is treated with Fe-BTC/PDA-42. The initial metal concentration is shown in grey and the final concentration after treatment with composite in distilled water and distilled water spiked with 100 ppm humic acid, is shown in blue and purple, respectively. No decrease in capacities is observed indicating no fouling.

pH Study

The elevated capacities observed in the Rhone river compared to distilled water is likely due to elevated pH in the fresh water source. Therefore, the effect of pH on the capacities of the material was evaluated. The pH was measured using a Hanna instruments Edge Multiparamter HI2020 pH meter. Solutions with concentrations of randing from 10 to 1000 ppm Hg^{2+} and Pb^{2+} were prepared and the pH was adjusted using 0.02M aqueous solutions of HCl and NaOH. About 10 mg of Fe-BTC/PDA-19 were added after a desired pH was reached and the pH was remeasured. The vials were placed in a Thermo Scientific MaxQ4450 Orbital Shaker for 24 hours at 200 rpms and held at a constant temperature of 28 °C. The samples were filtered using a 25 mm hydrophilic PTFE membrane syringe filter with 0.22 µm pores to remove any solids for elemental analysis of the aqueous media. It was observed that a higher initial pH will increase the capacities for both Hg^{2+} and Pb^{2+}. It should be noted that pH values below 3 lead to a decomposition of the MOF and at pH values above 8 to a precipitation of the metal salts. As such, the activity was only probed between 3 -7 for both Pb^{2+}, and Hg^{2+}.

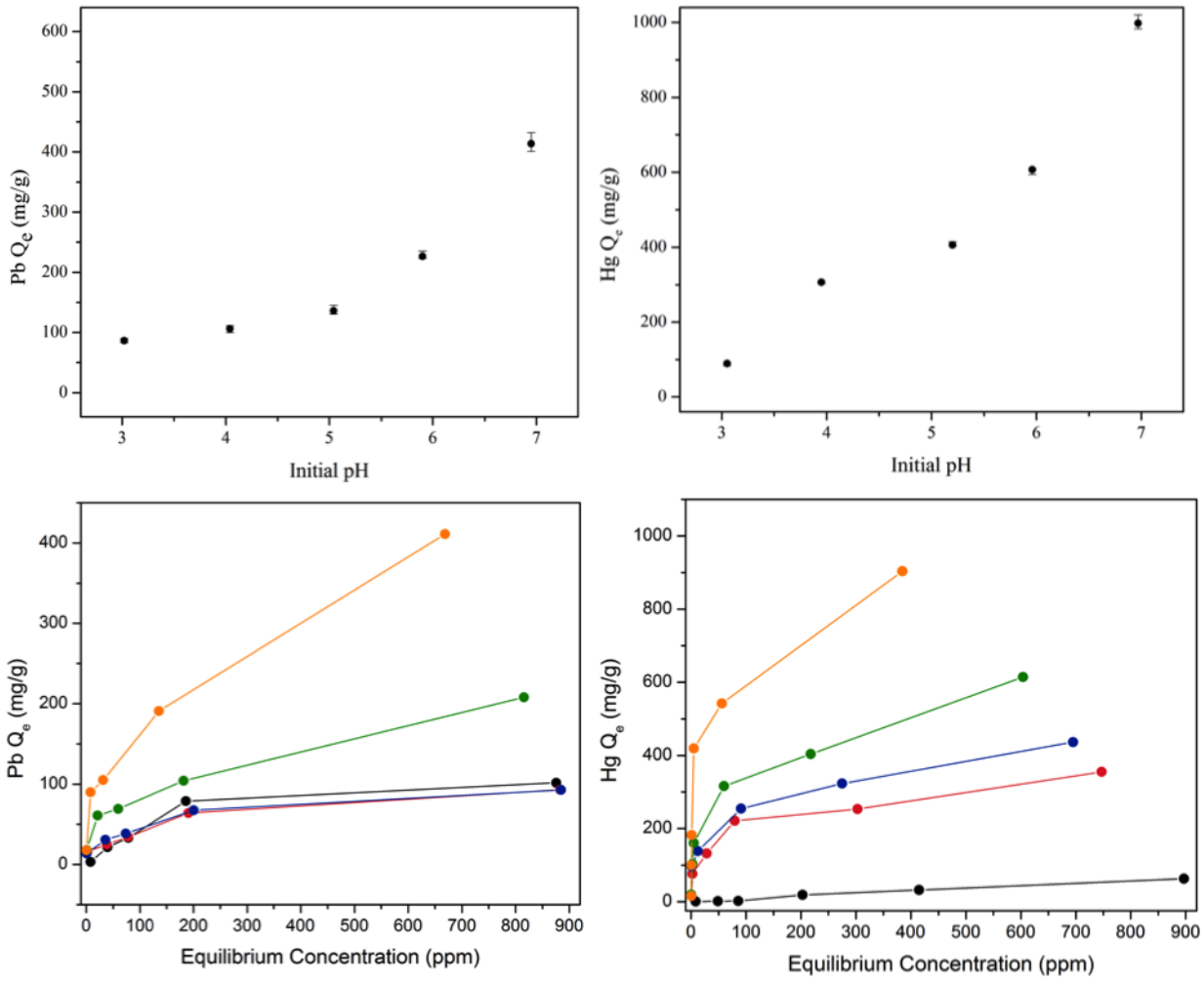

Figure S18 | Scatter plots showing Pb^{2+} (left) and Hg^{2+} (right) capacities (Q_e, mg/g) at pH values 3 (black), 4 (red), 5 (blue), 6 (green) and 7 (orange).

Recovery of Lead

Regeneration of the composite for Pb^{2+} was achieved using the reagent EDTA (ethylenediaminetetraacetic acid). For this experiment, 0.500 g of Fe-BTC/PDA-19 was added to 1000 ppm 1 liter aqueous solutions of Pb^{2+} to saturated the samples. After 24 hours, the samples were filtered, dried, and weighed. The Pb^{2+} concentrations in the aqueous media were analyzed and the values were used to calculate the capacity value Q_e (mg/g). The samples were added to 0.001 M solutions of EDTA acid and allowed to shake at 200 rpms for 4 hours. The samples were filtered, washed with methanol, dried and weighed. The EDTA regeneration solution was made into a 2 % HNO_3 solution for analysis to obtain the Pb^{2+} concentration to calculate the % recovery of Pb^{2+}. The regenerated materials were then added to 1000 ppm solutions of Pb^{2+} $^{+}$. This procedure was repeated 3 more times to obtain the Pb^{2+} percent recovery for each of the 4 cycles.

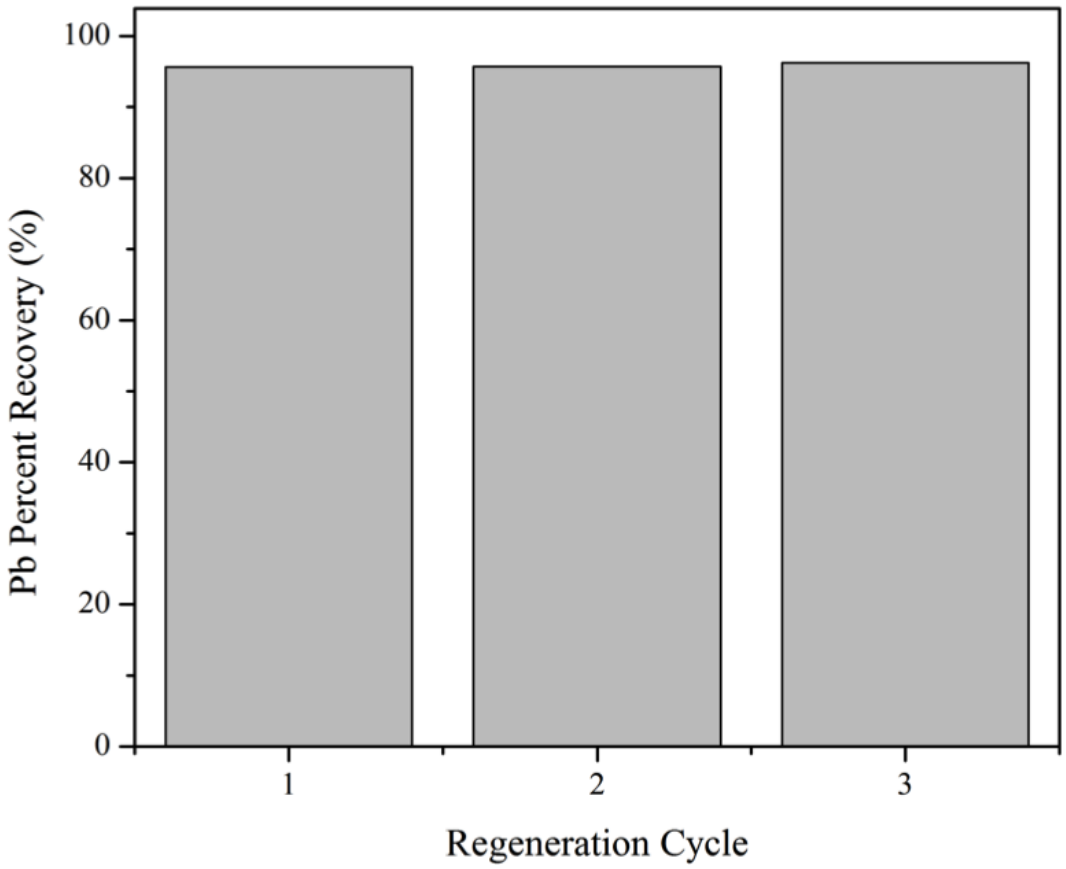

Figure S19 | After each regeneration cycle >95% of Pb^{2+} was recovered from the composite using EDTA.

Powder X-ray Diffraction pattern supporting the Reduction of Hg^{2+} to Hg^{1+}

After soaking Fe-BTC/PDA in a concentrated Hg^{2+} solution we performed powder x-ray diffraction on the resulting powder. We observe peaks that correlate to Hg_2Cl_2, which is the reduced form of $HgCl_2$. We surmise that the polymer's functional groups are reducing Hg from the 2+ to 1+ oxidation state.

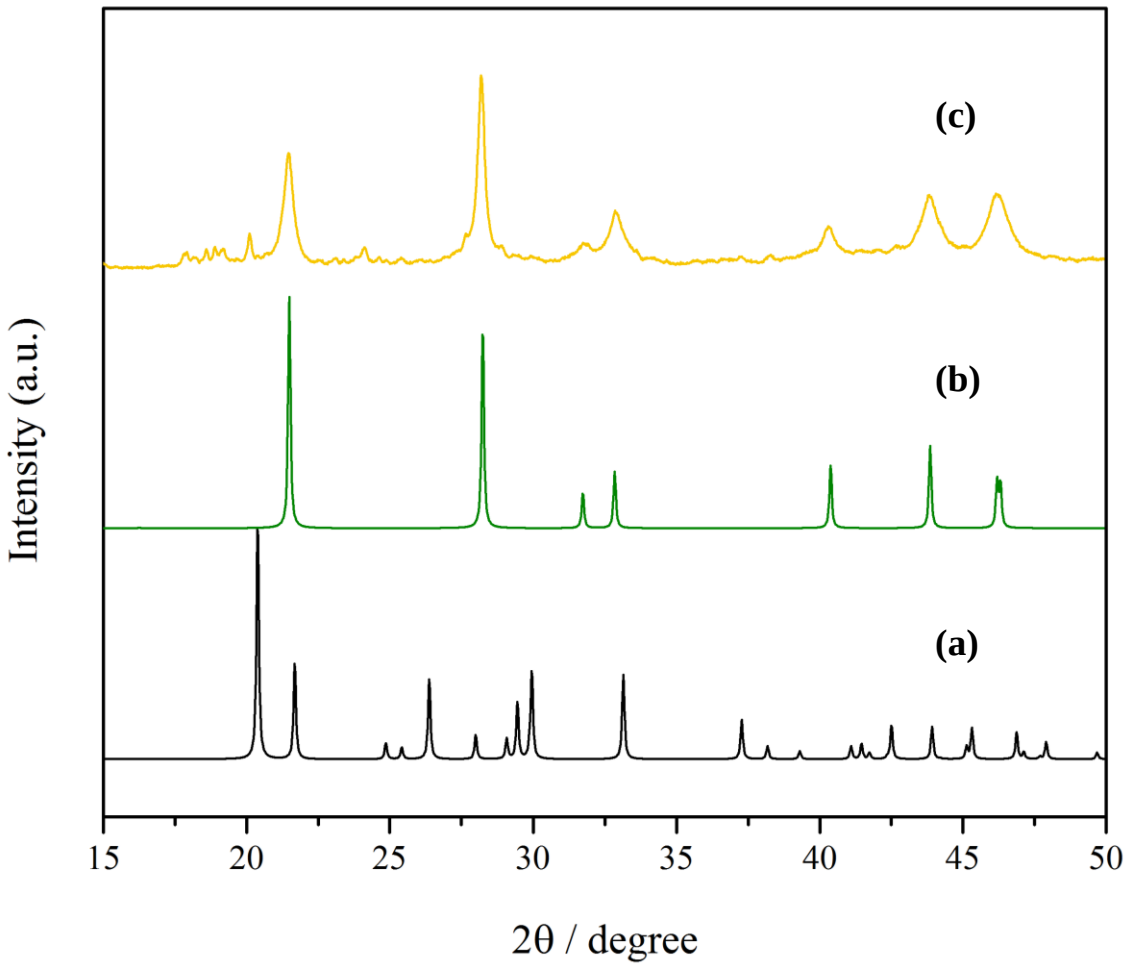

Figure S20 | Powder X-ray diffraction pattern of Fe-BTC/PDA-19 after being soaked in 1000 ppm solution of $HgCl_2$. (a) simulated pattern of $HgCl_2$ (b) simulated pattern of Hg_2Cl_2 and (c) experimental pattern of Fe-BTC/PDA-19 soaked in $HgCl_2$.

X-ray Photoelectron Spectroscopy

The C1 X-ray photoelectron spectrum for Fe-BTC-/PDA-19 fit for O-C=O, C-O, C-N, CH_x and $C-NH_2$ functional groups, which are present in MOF-Polymer composite and the O1 spectra fit for the functional groups O-C and HO-C. After soaking Fe-BTC/PDA in highly concentrated solutions of Hg^{2+} and Pb^{2+}, we looked to XPS to elucidate the electronic structure. We observe two signature peaks that fit the data for $HgCl_2$ and Hg_2Cl_2 or HgO. We surmise that the polymer is reducing the Hg^{2+} to Hg^{1+}. For Pb^{2+}, we also observe two signature peaks that fit the data for $Pb(OAc)_2$ and $Pb(OH)_2$. Curve fitting was performed using CasaXPS software[34].

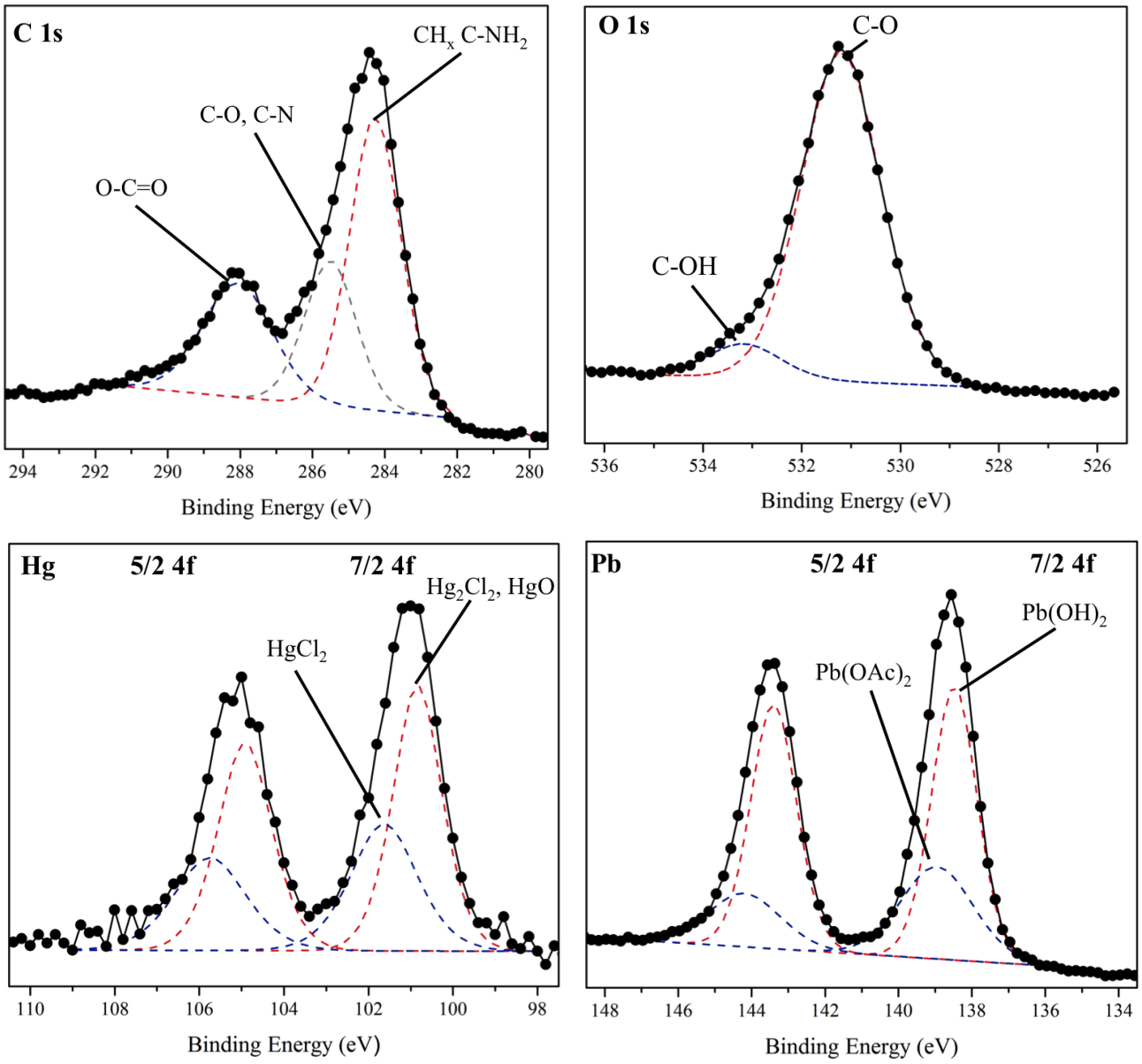

Figure S21 | X-ray photoelectron spectra of Fe-BTC/PDA-19 after soaking in Hg^{2+} or Pb^{2+} solutions. Values are specified in Table S3.

Performance in Real World Samples

Removal rate was measured in real world samples spiked with Pb^{2+} and Hg^{2+}. Common interferents such as Ca^{2+}, Na^{+} or organics can hinder the composite's removal efficiency and rate. Various vials containing 20 mL of Rhone River water , Mediterranean Sea and wastewater spiked with Pb^{2+} and Hg^{2+} were treated with 10 mg of Fe-BTC or Fe-BTC/PDA. At each time point, the samples were filtered using a 25 mm hydrophilic PTFE membrane syringe filter with 0.22 μm pores to remove any solids for elemental analysis of the aqueous media.

In a second experiment, a syringe was filled with 0.250 gram of Fe-BTC/PDA and 20 mL of ~0.8 ppm Pb^{2+} in Rhone river water or ~0.55 ppm of Pb^{2+} in Mediterranean Sea water was syringed through the samples. In all experiments Fe-BTC/PDA is able to reduce the concentration of Pb to drinkable levels illustrating the composites applicability to be used in real world applications.

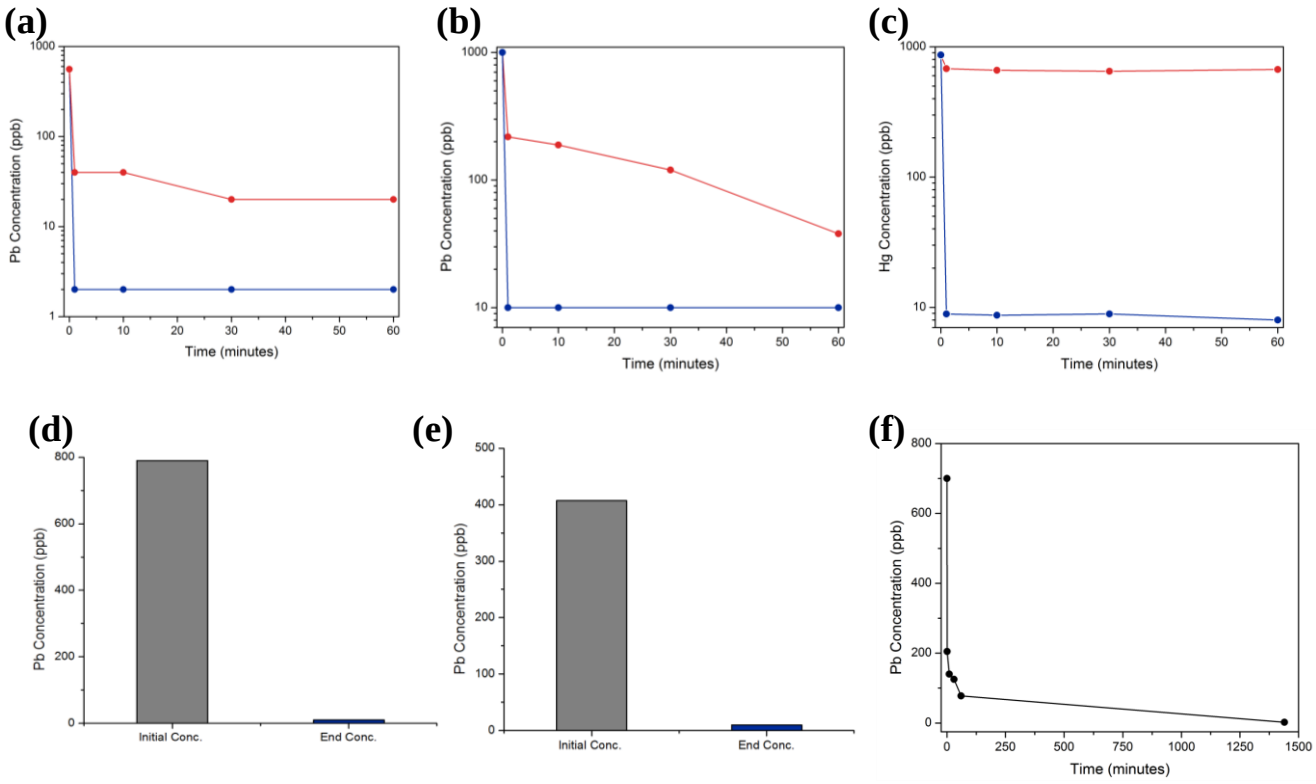

Figure S22 | Metal ion concentrations after treating Rhone River (a,c) and Mediterranean Sea (b) water contaminated with Pb^{2+} and Hg^{2+} with Fe-BTC/PDA-19 (blue) and Fe-BTC (red) at different time points. Equilibrium of the composite is reached by 1 minute. The initial and final concentration of Pb^{2+} in (d) Rhone River water and (e) Mediterranean Sea water after the contaminated solution is pushed through a syringe containing Fe-BTC/PDA, illustrating heavy metal removal in seconds and (f) the removal rate of Fe-BTC/PDA in wastewater from a treatment facility spiked with Pb^{2+}.

Heavy Metal Removal with Increasing PDA Loading

Composites containing various amount of PDA, ranging from 19 to 42 mass %, were added to concentrated solutions of Hg^{2+} (1000 ppm) to assess the effect of the polymer loading on heavy metal removal, Q_e (mg/g). The mixtures were transferred to a Thermo Scientific MaxQ4450 Orbital Shaker for 24 hours at 200 rpms and held at a constant temperature of 28 °C. The samples were filtered using a 25 mm hydrophilic PTFE membrane syringe filter with 0.22 μm pores to remove any solids for elemental analysis of the aqueous media. After the analysis, Q_e, the amount of metal removed per gram of composite (mg/g), was calculated using the equation above.

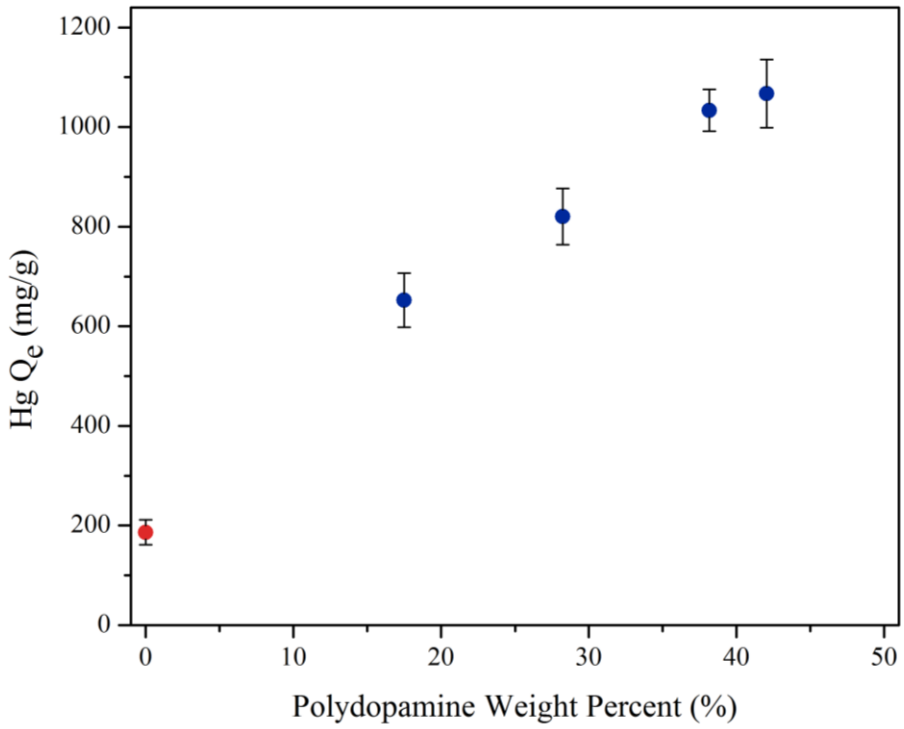

Figure S23 | Hg^{2+} capacities in distilled water plotted against polydopamine loading in Fe-BTC. For the experiments the MOF was loaded with various amounts of polydopamine ranging from 0 to ~45 mass percent.

Performance of Different Composites in Real World Samples

Different composites were evaluated for Pb^{2+} removal from Rhone River water. 50 mg of composite was loaded into a syringe with a 25 mm hydrophilic PTFE membrane syringe filter of 0.22 µm pores. 10 mL of the of the contaminated river water was passed through and the solution was analyzed to measure the Pb^{2+} concentration.

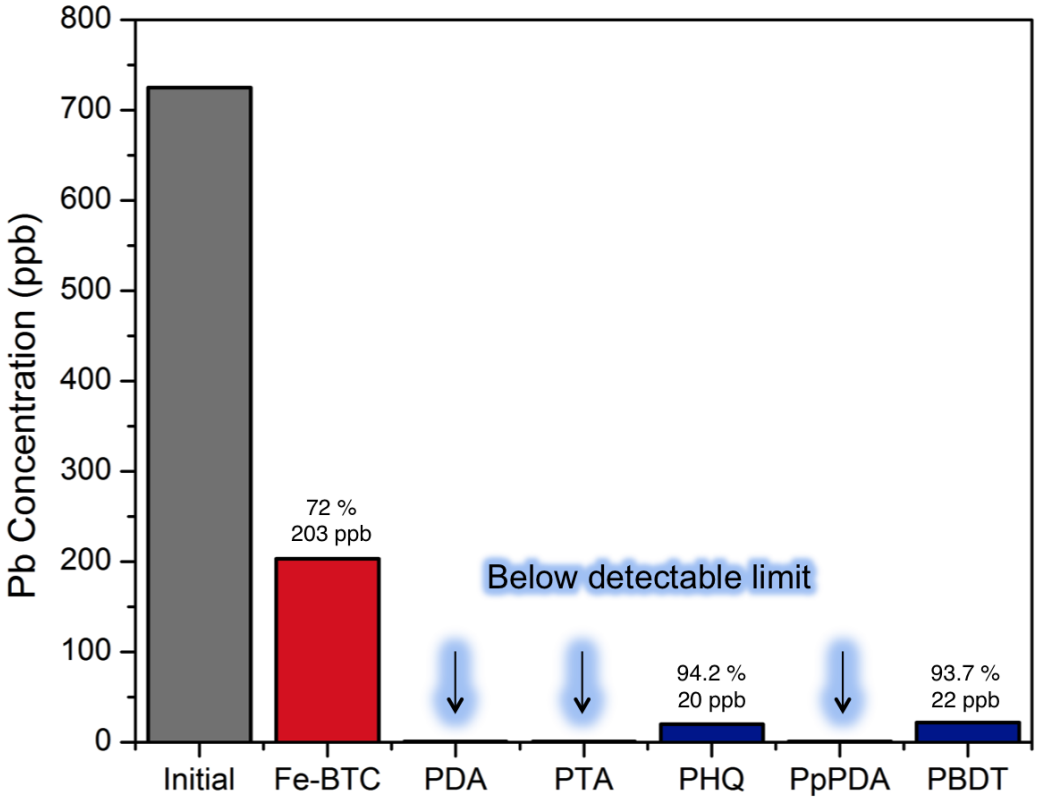

Figure S24 | Pb^{2+} concentrations after treating Rhone River water with different composites.

Table S1
The dopamine equivalence and concentrations with its C H N % values from the combustion analysis. The polydopamine mass % was calculated based on the N %.

Dopamine:Fe_3	Dopamine Concentration (mM)	C%	H%	N%	PDA% (based on N%)	BET Surface Area (m^2/g)
2.5	12	39.55	2.45	1.81	19.05	1134
5.0	24	42.55	2.98	3.01	28.21	757
7.5	36	47.97	3.86	4.73	38.15	488
10	47	49.67	4.39	5.57	42.05	165

Table S2
The binding energies (kcal/mol) and binding distances (Å) for the functional groups of possible polydopamine derivatives to the Fe metal site on the SBUs (secondary building unit)

ID	PDA structure	Binding site	Binding energy ($\frac{kcal}{mol}$)	Binding distance (Å)
1		N	-29.4	2.3
		O	-20.4	2.1
2	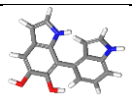	N	-26.3	3.1
		O	-28.4	2.2
4	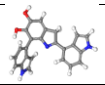	N	-23.3	3.6
5		N	-40.2	1.9
		O	-18.8	2.3
6	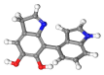	N	-36.6	2.1
		O	-27.2	2.2
7		O	-29.0	2.0
		N	-28.2	2.3
8	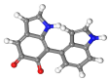	O	-33.7	2.0
		N	-27.7	3.2
9		O1	-23	2.0
		O2	-17.3	2.2
		N	-21.8	2.7
10	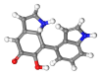	O1	-18.2	2.3
		N	-25.8	3.2
11	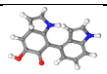	O2	-26.5	2.0
12	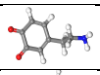	N	-39.3	2.1
13	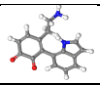	O	-33.8	2.0
14		O	-23.1	2.2
		N	-41.97	2.1
15	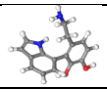	O	-24.0	2.2

Table S3
The binding energy values from the XPS for each functional group present within the composite.

Functional Group	Binding Energy (eV)
Hg_2Cl_2, HgO	100.8
$HgCl_2$	101.6
$Pb(OH)_2$	138.4
$Pb(OAc)_2$	138.9
CH_x, C-NH_2	284.4
C-O, C-N	285.4
O-C=O	288.3
C=N-C	399.4
C_2NH	400.4
C-NH_2	402.0
O-C	531.2
HO-C	533.2

Table S4 Top performing materials for lead removal

Material	Surface Area (m^2/g)	Mechanism	Reach EPA of ~10 ppb with soaking?	Speed to EPA limit (min.)	Pb^{2+} Capacity (mg/g)	k_d (mL/g)	Regenera-tion	Organic Interferent Test	Selective over Na^+, Ca^{2+}, Mg^{2+}	Ref.
Fe-BTC	2300	Adsorption	✗[a]	✗	162	3.5×10^2	N.R.[b]	✔[a]	N.R.	This work
Fe-BTC/PDA	1134	Adsorption	✔	< 1	394	1.7×10^6	✔	✔	✔	This work
DPA-LDH[c]	168.3	Adsorption	✔	~ 40	479	1.99×10^8	N.R.	N.R.	N.R.	2
MoS_4-LDH[d]	N.R.	Adsorption	✔	> 30	290	2.6×10^5	N.R.	N.R.	N.R.	1
$Zn_3L_3(BPE)_{1.5}$[e]	82.5	Adsorption	✗	✗	616.6	2.3×10^6	✔	N.R.	✔	3
mPMF[f]	1099	Adsorption	✔	1	0.628	N.R.	✔	N.R.	✔	20
PDA-Ms[g]	N.R.	Adsorption	✔	N.R.	160	2.39×10^3	✔	N.R.	✔	5
68W[h]	18.1	Adsorption	✗	✗	254.1	3.17×10^5	N.R.	N.R.	N.R.	7
chitosan/PEI[i]	N.R.	Adsorption	✔	~ 40	341	N.R.	✔	N.R.	✔	21
PbIMS[j]	762	Adsorption	✗	✗	160	2.97×10^3	✔	N.R.	✔	4
ED-MIL-101-Cr[k]	347	Adsorption	✗	✗	81.09	1.18×10^3	✔	N.R.	N.R.	22
MgO@N-biochar[l]	83.2	Ion-exchange	✗	✗	893	N.R.	✔	✔	✔	24
MgO Flower[m]	72	Ion-exchange	✔	> 60	1980	N.R.	N.R.	N.R.	N.R.	25
001x7[n]	N.R.	Ion exchange	✔	N.R.	434.7	4.9×10^4	N.R.	N.R.	✔	5
K-MPS-1[o]	N.R.	Ion-exchange	✔	> 720	393.5	5.36×10^5	N.R.	N.R.	✔	6

highlighted boxes (in yellow) represent excellent performance for a specific metric.

a. **x** implies it was not achieved under the conditions tested. ✔ indicates this parameter was tested and shows reasonable performance.

b. N. R. implies that the parameter is not reported and could not be calculated from the presented data.

c. DPA-LDH is a Ni/Cr Layered double hydroxide with diphenylamine-4-sulfonate intercalated within the layers. While the material reaches the EPA limit in DI water, it takes ~ 40 minutes to reach this. Further, selectivity tests for mixtures containing equivalent amounts of Pb^{2+} Cd^{2+}, Cu^{2+}, and Zn^{2+}, were carried out. Despite that the material adsorbs all 4 metals, it still manages to get to the EPA limit for Pb^{2+}, but it takes 60 minutes. No tests were performed against other important interferents like Na^+, Mg^{2+}, or Ca^{2+} found in real world water samples.

d. MoS_4-LDH is a layered double hydroxide with MoS_4^{2-} anions intercalated in between the layers. While selectivity tests are carried out with equivalent amounts of several ions including Ni^{2+}, Co^{2+}, Cu^{2+}, Zn^{2+}, Ag^+, Pb^{2+}, Cd^{2+}, and Hg^{2+}, it is shown to absorb significant amounts of all metals except Co^{2+}, Ni^{2+}, Zn^{2+}, and Cd^{2+}, Further, it does not get anywhere close to reaching the EPA limit for Pb^{2+} under these conditions within a 3 hour window (reaches only ~ 650 ppb). No tests were done to see how the materials perform in natural water samples with large amounts of Na^+, Ca^{2+}, or Mg^{2+} nor is there any information pertaining to recyclability.

e. $Zn_3L_3(BPE)_{1.5}$ is a Zn-containing MOF (where L^{2-} = 4,4'-azoxydibenzate and BPE = bis(4-pyridyl)ethylene). While the material has a higher capacity, it is not able to get to the EPA limit under the reported conditions listed. From 10 ppm Pb^{2+} concentration reaches approximately 35 ppb in an hour, which is the equilibration time. The material equilibrium is quite slow compared to Fe-BTC/PDA, likely due to the structural transformation it undergoes. The material is not tested in real world water samples, but does show high selectivity for Pb^{2+} over Na^+, Ca^{2+}, and Mg^{2+}, having ratios up to 1:50 (10 ppm Pb : 500 ppm mixed ions). The materials stability is only tested for 300 minutes. Last, the material is cycleable but shows a drop by 10 to 15 % in cycles 3 and 4.

f. MPMF is a mesoporous poly-melamine-formaldehyde polymer: Until Fe-BTC/PDA, this polymer is the fastest reported to date to the EPA limit, but it has extremely low capacities. As such, large amounts of material is required and it only operates well when the concentrations of the solutions are already well into the ppb regime, 50 to 100 ppb of Pb^{2+}.

g. PDM-Ms are polydopamine microspheres. It is expected that these should perform similarly to Fe-BTC/PDA, however it can be seen that the k_d is much higher for our composite and this material is not shown to get below the EPA limit; however, the equilibrium time is on the order of a minute.

h. Porous Indium Sulfide (68W) was generated using an In-MOF known as MIL-68 or In(BDC)OH treated with Na_2S in water. No information is given with regard to testing the selectivity of the material in sources contaminated with other metals. It also is not reported that it reaches the EPA limit and no information is given with regard to equilibrium times.

i. This polymer is a magnetic gelatin that consists of chitosan grafted PEI (polyethylene imine). The cationic polymer can only reach the EPA limit from extremely low concentrations, ~200 ppb. Further, it is regenerable in 0.1 mmol/L Acetic Acid; however, the removal efficiency drops to 89% over 5 cycles. Last, the cationic polymer adsorbs most cations and anions found in drinking water, which decrease the efficiency, particularly Ca^{2+}. Last, it should be noted that the capacity is determined by fitting adsorption isotherms, actually capacities above 66 mg/g for Pb^{2+}were never measured.

j. PbIMS is an periodic ion imprinted silica, SBA-15. Despite that equilibrium is reached in short times, approximately 7 minutes at low concentrations, they do not show under the conditions tested that the material is capable of getting below the EPA limit. While they show the material is selective for various ions such as Na^+, K^+, Ca^{2+}, Mg^{2+}, Cu^{2+}, and Cd^{2+}, they also show that the material is still adsorbing a significant amount of some of these ions from solution, particularly K^+.

k. ED-MIL-101 is an ethylene diamine grafted to the metal sites in the MOF. It has a capacity that drops off by 50% after 4 cycles, likely indicating loss of the amines.

l. MgO@Nbiochar is not shown to get below the EPA limit but removal efficiencies approach 99% in 10 minutes.

m. MgO Flower: Despite high capacities, no selectivity is illustrated. Further, the material reaches the EPA limit, but it can only be done from very low starting concentrations of 200 ppb and very long equilibrium times that are longer than 60 minutes.
n. 001x7[h] is a commercial ion exchange resin.
o. K-MPS-1 is a potassium intercalated layered metal thiophosphate, with the formula $K_{0.48}Mn_{0.76}PS_3 \cdot H_2O$. It is reported to get below the EPA limit but only at very low starting concentrations and long soak times compared to Fe-BTC/PDA. Full equilibration times are reported to be on the order of 2 days. Last, while they tested to see if the Pb^{2+} could be removed, they have not shown that the materials properties

Table S5 Top performing materials for mercury removal

Material	Surace Area (m^2/g)	Mechanism	Reach EPA of ~10 ppb with soaking?	Speed to EPA limit (min.)	Hg^{2+} Capacity (mg/g)	K_d (mL/g)	Regenera -tion	Organic Interferent Test	Selective over Na^+, Ca^{2+}, Mg^{2+}	Ref.
Fe-BTC	2300	Adsorption	✗[a]	✗	210	3.5×10^2	N.R.[b]	✔[a]	N.R.	This work
Fe-BTC/PDA	1134	Adsorption	✔	< 1	1670	5.5×10^6	✔	✔	✔	This work
68W[c]	18.1	Adsorption	✗	✗	2170	6.9×10^6	N.R.	N.R.	N.R.	7
TPB-DMTP-COF-SH[d]	291	Adsorption	✔	~10	4395	3.23×10^9	✔	N.R.	✔	17
NanoSe Sponge[e]	N.R.	Adsorption	✔	~10	624	1.67×10^9	✗	N.R.	✔	16
COF-S-SH[f]	496	Adsorption	✔	~20	1350	2.3×10^9	✔	N.R.	✔	18
PAF-1-SH[g]	3274	Adsorption	✔	~30	1000	5.76×10^7	✔	N.R.	✔	13
BioMOF[h]	N.R.	Adsorption	✗	✗	900	N.R.	N.R.	N.R.	✔	14
S-FMC-900[i]	1400	Adsorption	✗	✗	732	5.13×10^5	N.R.	N.R.	N.R.	9
Zr-DMBD[j]	513	Adsorption	✗	✗	140.6	N.R.	N.R.	N.R.	N.R.	12
LMOF-263[k]	1004	Adsorption	✗	✗	380	6.45×10^5	N.R.	N.R.	✔	15
DMS-Fe_3O_4[l]	114	Adsorption	✗	✗	227	2.8×10^5	N.R.	N.R.	✔	10
LHMS-1[m]	N.R.	Ion Exchange	✔	~2	87	6.41×10^6	✔	N.R.	N.R.	11

highlighted boxes (in yellow) represent excellent performance for a specific metric.

a. x implies it was not achieved under the conditions tested. ✔indicates this parameter was tested and shows reasonable performance.
b. N. R. implies that the parameter is not reported and could not be calculated from the presented data.
c. Porous Indium Sulfide (68W) was generated using an indium-MOF known as MIL-68 or In(BDC)OH treated with Na_2S in water. No information is given with regard to testing the selectivity of the material in sources contaminated with other common metals. It also is not reported that it reaches the EPA limit and no information is given with regard to equilibrium times. Further, it should be noted that indium is not only toxic, but also highly expensive.
d. TPB-DMTP-COF-SH is a covalent organic framework functionalized with pendant thiol groups. While the material performs well in DI water, its removal efficiency is reduced by over 20% when in the presence of common inorganics like, Ca^{2+}, Na^+, and Mg^{2+}. It should be noted that the materials can reportedly get to the EPA limit but 20 mg of sample is placed in 1 mL of solution 10 ppm solution. This test is rather unrealistic. Comparatively, FeBTC/PDA can do the same job with significantly less sample and at least ten times faster.
e. The nano selenium sponge is one of the best materials reported for Hg removal. The Hg^{2+} concentration is reduced to the ppt regime in seconds. However, this is only done under pressure, and the authors do not report what is the length of time that they wait for the water to diffuse into the sponge. Further, they use 30 times more material and are unable to reach the EPA limit within a 10 minute window when just soaking the material in water, as done in our experiments. Also, the material is not reversible. While this is good for in home treatment, it can be seen as a big disadvantage for wastewater treatment.
f. COF-S-SH is a covalent organic framework. While the material is shown to be selective in the presence of Mg^{2+} and Ca^{2+}, there is no report of Na^+. Further, significant amounts of the common ions are shown to adsorb and the manuscript gives no indication of the actual concentrations to show that these materials selectively bind Hg^{2+} at low concentrations while in the presence of high concentrations of these other inorganics.
g. PAF-1-SH, also referred to as the mercury nanotrap, is a porous organic polymer. It can be regenerated with only about a 10% loss in removal efficiency in 3 cycles. They show that in the presence of Ca^{2+}, Na^+, and Mg^2that the material maintains Hg^{2+} capacity; however, they do not report on the removal rate with these other ions and they also do not test in high concentrations of the other ions. They start with 3 ppm Hg^2+ and 0.61, 0.36, and 8.22 ppm of Ca^{2+}, Mg^{2+}, and Na^+ respectively. It should be noted that the concentrations of the competing ions should be significantly higher, (and low concentrations of Hg^{2+}) as expected for wastewater, to truly test selectivity.
h. BioMOF is a MOF with the formula $CaCu_6[(S,S)\text{-methox}]_3(OH)_2(H_2O)\}\cdot 16H_2O$ that is decorated with thioalkyl chains. The material is reported to be selective for $Hg2^+$ over Na^+, K^+, Ca^{2+}, and Mg^{2+}; however, it should be noted that the solutions contained 10 ppm of all ions. They were not tested in high concentrations of these ions with low concetrnations of Hg^{2+}, which is more realistic for wastewater. Further, there are no other experimental procedures that describe whether the other ions are adsorbed nor if the same removal efficiency is achieved with Hg^{2+} in their presence.
i. S-FMC is a sulfur-functionalized mesoporous carbon.
j. Zr-DMBD is a thiol-laced MOF (where $DMBD^{2-}$ = 2,5-dimercapto-1,4-benzenedicarboxyate)

k. L-MOF-263 is a luminescent metal−organic framework with the chemical formula, $Zn_2(dbtdcO_2)_2(tppe)$ where ($dbtdcO_2$) = [dibenzo[b,d]thiophene-3,7-dicarboxylate 5,5-dioxide] and tppe = 1,1,2,2-tetrakis(4-(pyridine-4-yl)phenyl)ethane. For selectivity, L-MOF was only tested in the presence of Mg^{2+} and Ca^{2+}, not Na^{+}. Further, the concentrations were equivalent, (10 ppm for all M^{2+}) rather than low concentrations of Hg and high concentrations of these competing ions. While they report the luminescent properties are reproducible with cycling, they do not actually show that the material can be fully regenerated and cycled.
l. DMS-Fe_3O_4 contains Fe_3O_4 nanoparticles functionalized with dimercaptosuccinic acid (DMSA).
m. LHMS-1 is a layered hydrogen metal sulfide with the chemical formula $H_{2x}Mn_xSn_{3-x}S_6$ (x ¼ 0.11–0.25). It should be noted that while the material works in 2 minutes, it is only tested in 67 ppb solutions. Further, 1 gram of LHMS is used per 1L of water. For Fe-BTC/PDA, half as much material is employed, and it was able to reduced 1000 ppb to drinkable conditions in less than a minute.

Table S6
BET surface areas and polymer loadings of different composites

Composite	Polymer Building Unit	BET Surface Area (m^2/g)	Polymer Mass %
Fe-BTC/PTA	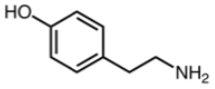	1665	14.31
Fe-BTC/PHQ	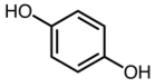	1767	19.69
Fe-BTC/PpPDA	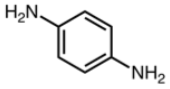	1032	21.1
Fe-BTC/PmAP	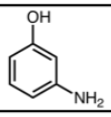	1488	16.54
Fe-BTC/PBDT	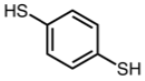	683	10.21
Cu-TDPAT/PDA	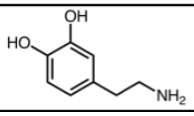	434	24.11

References

1. Ma, L.; Wang, Q.; Islam, S. M.; Liu, Y.; Ma, S.; Kanatzidis, M. G., Highly Selective and Efficient Removal of Heavy Metals by Layered Double Hydroxide Intercalated with the MoS_4^{2-} Ion. *J. Am. Chem. Soc.* **2016,** *138* (8), 2858-2866.
2. Asiabi, H.; Yamini, Y.; Shamsayei, M.; Tahmasebi, E., Highly selective and efficient removal and extraction of heavy metals by layered double hydroxides intercalated with the diphenylamine-4-sulfonate: A comparative study. *Chem. Eng. J.* **2017,** *323*, 212-223.
3. Hou, H.; Yu, C.-X.; Shao, C. Z., A functionalized metal-organic framework decorated with O- groups showing excellent performance for lead(II) removal from aqueous solution. *Chem. Sci.* **2017,** 8, 7611-7619.
4. He, R.; Li, W.; Deng, D.; Chen, W.; Li, H.; Wei, C.; Tang, Y., Efficient removal of lead from highly acidic wastewater by periodic ion imprinted mesoporous SBA-15 organosilica combining metal coordination and co-condensation. *J. Mater. Chem. A* **2015,** *3* (18), 9789-9798.
5. Zhang, Q.; Yang, Q.; Phanlavong, P.; Li, Y.; Wang, Z.; Jiao, T.; Peng, Q., Highly Efficient Lead(II) Sequestration Using Size-Controllable Polydopamine Microspheres with Superior Application Capability and Rapid Capture. *ACS Sustain Chem Eng* **2017,** *5* (5), 4161-4170.
6. Rathore, E.; Pal, P.; Biswas, K., Layered Metal Chalcophosphate (K-MPS-1) for Efficient, Selective, and ppb Level Sequestration of Pb from Water. *J. Phys. Chem. C* **2017,** *121* (14), 7959-7966.
7. Abney, C. W.; Gilhula, J. C.; Lu, K.; Lin, W., Metal-Organic Framework Templated Inorganic Sorbents for Rapid and Efficient Extraction of Heavy Metals. *Adv. Mater.* **2014,** *26* (47), 7993-7997.
8. Gunathilake, C.; Kadanapitiye, M. S.; Dudarko, O.; Huang, S. D.; Jaroniec, M., Adsorption of Lead Ions from Aqueous Phase on Mesoporous Silica with P-Containing Pendant Groups. *ACS Appl. Mater. Interfaces* **2015,** *7* (41), 23144-23152.
9. Shin, Y.; Fryxell, G. E.; Um, W.; Parker, K.; Mattigod, S. V.; Skaggs, R., Sulfur-Functionalized Mesoporous Carbon. *Adv. Funct. Mater* **2007,** *17* (15), 2897-2901.
10. Yantasee, W.; Warner, C. L.; Sangvanich, T.; Addleman, R. S.; Carter, T. G.; Wiacek, R. J.; Fryxell, G. E.; Timchalk, C.; Warner, M. G., Removal of Heavy Metals from Aqueous Systems with Thiol Functionalized Superparamagnetic Nanoparticles. *Sci. Total Environ.* **2007,** *41* (14), 5114-5119.
11. Manos, M. J.; Petkov, V. G.; Kanatzidis, M. G., H2xMnxSn3-xS6 (x = 0.11–0.25): A Novel Reusable Sorbent for Highly Specific Mercury Capture Under Extreme pH Conditions. *Adv. Funct. Mater* **2009,** *19* (7), 1087-1092.
12. Yee, K.-K.; Reimer, N.; Liu, J.; Cheng, S.-Y.; Yiu, S.-M.; Weber, J.; Stock, N.; Xu, Z., Effective Mercury Sorption by Thiol-Laced Metal–Organic Frameworks: in Strong Acid and the Vapor Phase. *J. Am. Chem. Soc.* **2013,** *135* (21), 7795-7798.
13. Li, B.; Zhang, Y.; Ma, D.; Shi, Z.; Ma, S., Mercury nano-trap for effective and efficient removal of mercury(II) from aqueous solution. *Nat. Commun.* **2014,** *5*, 5537.
14. Mon, M.; Lloret, F.; Ferrando-Soria, J.; Martí-Gastaldo, C.; Armentano, D.; Pardo, E., Selective and Efficient Removal of Mercury from Aqueous Media with the Highly Flexible Arms of a BioMOF. *Angew. Chem. Int. Ed* **2016,** *55* (37), 11167-11172.
15. Rudd, N. D.; Wang, H.; Fuentes-Fernandez, E. M. A.; Teat, S. J.; Chen, F.; Hall, G.; Chabal, Y. J.; Li, J., Highly Efficient Luminescent Metal–Organic Framework for the Simultaneous Detection and Removal of Heavy Metals from Water. *ACS Appl. Mater. Interfaces* **2016,** *8* (44), 30294-30303.
16. Ahmed, S.; Brockgreitens, J.; Xu, K.; Abbas, A., A Nanoselenium Sponge for Instantaneous Mercury Removal to Undetectable Levels. *Adv. Funct. Mater* **2017,** *27* (17), 1606572-n/a.
17. Meri-Bofi, L.; Royuela, S.; Zamora, F.; Ruiz-Gonzalez, M. L.; Segura, J. L.; Munoz-Olivas, R.; Mancheno, M. J., Thiol grafted imine-based covalent organic frameworks for water remediation through selective removal of Hg(ii). *J. Mater. Chem. A* **2017,** *5* (34), 17973-17981.
18. Sun, Q.; Aguila, B.; Perman, J.; Earl, L. D.; Abney, C. W.; Cheng, Y.; Wei, H.; Nguyen, N.; Wojtas, L.; Ma, S., Postsynthetically Modified Covalent Organic Frameworks for Efficient and Effective Mercury Removal. *J. Am. Chem. Soc.* **2017,** *139* (7), 2786-2793.
19. Horcajada, P.; Surble, S.; Serre, C.; Hong, D.-Y.; Seo, Y.-K.; Chang, J.-S.; Greneche, J.-M.; Margiolaki, I.; Ferey, G., Synthesis and catalytic properties of MIL-100(Fe), an iron(iii) carboxylate with large pores. *Chem. Commun* **2007,** (27), 2820-2822.
20. Tan, M. X.; Sum, Y. N.; Ying, J. Y.; Zhang, Y., A mesoporous poly-melamine-formaldehyde polymer as a solid sorbent for toxic metal removal. *Energy Environ. Sci.* **2013,** *6* (11), 3254-3259.

21. Li, B.; Zhou, F.; Huang, K.; Wang, Y.; Mei, S.; Zhou, Y.; Jing, T., Environmentally friendly chitosan/PEI-grafted magnetic gelatin for the highly effective removal of heavy metals from drinking water. *Sci Rep*. **2017,** *7*, 43082.
22. Luo, X.; Ding, L.; Luo, J., Adsorptive Removal of Pb(II) Ions from Aqueous Samples with Amino-Functionalization of Metal–Organic Frameworks MIL-101(Cr). *J. Chem. Eng. Data* **2015,** *60* (6), 1732-1743.
23. *Mnova NMR*, Mestrelab Research 2016.
24. Ling, L.-L.; Liu, W.-J.; Zhang, S.; Jiang, H., Magnesium Oxide Embedded Nitrogen Self-Doped Biochar Composites: Fast and High-Efficiency Adsorption of Heavy Metals in an Aqueous Solution. *Environ.Sci. Technol.* **2017,** *51* (17), 10081-10089.
25. Cao, C.-Y.; Qu, J.; Wei, F.; Liu, H.; Song, W.-G., Superb Adsorption Capacity and Mechanism of Flowerlike Magnesium Oxide Nanostructures for Lead and Cadmium Ions. *ACS Appl. Mater. Interfaces* **2012,** *4* (8), 4283-4287.
26. Liebscher, J.; Mrówczyński, R.; Scheidt, H. A.; Filip, C.; Hădade, N. D.; Turcu, R.; Bende, A.; Beck, S., Structure of Polydopamine: A Never-Ending Story? *Langmuir* **2013,** *29* (33), 10539-10548.
27. Dreyer, D. R.; Miller, D. J.; Freeman, B. D.; Paul, D. R.; Bielawski, C. W., Elucidating the Structure of Poly(dopamine). *Langmuir* **2012,** *28* (15), 6428-6435.
28. Perdew, J. P.; Burke, K.; Ernzerhof, M., Generalized Gradient Approximation Made Simple. *Phys. Rev. Lett.* **1996,** *77* (18), 3865-3868.
29. Grimme, S., Semiempirical GGA-type density functional constructed with a long-range dispersion correction. *J. Comput. Chem.* **2006,** *27* (15), 1787-1799.
30. Poloni, R.; Smit, B.; Neaton, J. B., CO2 Capture by Metal–Organic Frameworks with van der Waals Density Functionals. *J. Phys. Chem. A* **2012,** *116* (20), 4957-4964.
31. Hendon, C. H.; Tiana, D.; Fontecave, M.; Sanchez, C.; D'arras, L.; Sassoye, C.; Rozes, L.; Mellot-Draznieks, C.; Walsh, A., Engineering the Optical Response of the Titanium-MIL-125 Metal–Organic Framework through Ligand Functionalization. *J. Am. Chem. Soc.* **2013,** *135* (30), 10942-10945.
32. Planas, N.; Dzubak, A. L.; Poloni, R.; Lin, L.-C.; McManus, A.; McDonald, T. M.; Neaton, J. B.; Long, J. R.; Smit, B.; Gagliardi, L., The Mechanism of Carbon Dioxide Adsorption in an Alkylamine-Functionalized Metal–Organic Framework. *J. Am. Chem. Soc.* **2013,** *135* (20), 7402-7405.
33. Li, B.; Zhang, Y.; Ma, D.; Shi, Z.; Ma, S., Mercury nano-trap for effective and efficient removal of mercury(II) from aqueous solution. *Nat. Commun.* **2014,** *5*, 5537.
34. *CasaXPS: Processing Software for XPS, AES, SIMS and More* Casa Software Ltd: 2016.